# STRUCTURAL MODE IDEN"1'IF'ICATION OF GALILEO SPACECRAFT FROM FLIGHT DATA

Che-Hang Charles lh, Shuh-Ren I in, Edward C. Wong and Glenn A. Macala

Jet Propulsion Laboratory
California Institute of Technology
Pasadena, California

## ABSTRACT

Due to the noncolocation of sensors and actuator for the Galileo clock control loop, an in-flight identification was performed to identify the stator structural resonance frequencies, mode shapes and damping ratios. This information was necessary to ensure the stability of and enhance the performance of the clock controller. "l'his Clock System identification (CLK SYSID) test was executed on-board on January 2.0, 1993. This paper presents the background, process, results and analysis of CLK SYSID. Some unexpected artifact modes at the multiples of 1.5 Hz showed up on the gyro rate Power Spectrum Density (PSD) plots, and the cause for that was hypothesized and demonstrated through simulation. It conclusion, the results showed that no significant stator flexible modes were excited using torque pulse inputs of various widths. Thus, no updates to the clock controller parameters were required,

## 1. INTRODUCTION

The Galileo spacecraft was launched in 1989 and is on its way to explore Jupiter, The dual-spin configured spacecraft will orbit Jupiter to conduct scientific investigation of the planet and its satellites. A probe will be released prior to Jupiter orbit insertion and will follow an impact trajectory for atmospheric investigation [1] [2.]. An illustration of the Galileo spacecraft is shown in Fig. 1.

The scan platform of the Galileo spacecraft is attached to a flexible stator structure (despun section) that is in turn attached to the rotor (spun section) of the spacecraft, "l'here at-e two degrees of freedom for controlling the inertial pointing of the scan platform. The clock actuator at the Spin Bearing Assembly (SBA) controls the relative position between the rotor and the stator, and the ccme actuator controls the relative position between the platform and the stator. The inertial sensors (gyros) arc located on the platform.

The cone actuator and the gyros are separated by a rigid platform structure, hence gyro measurements can be directly used by the cone. controller to generate cone actuation signals. The clock actuator, however, is separated from the gyros by the flexible stator structure. Because the sensors and actuator are noncolocated, the gyros sense flexible motion as well as rigid body motion. When the clock controller attempts to compensate the position error caused by the flexible vibration at the resonance frequencies, it may destabilize the system. Thus, a wide double-notch filter was imbedded into the clock controller design (see Fig. 2) to attenuate the control gain at the notch frequency and prevent the flexible motion from feeding back into the structure [3] [4]. I lowever, due to the high uncertainty in the ground NASTRAN model, an in-flight identification of the stator flexible mode characteristics (modal frequency, damping and coefficient) is necessary to accurately locate the "destabilizing frequencies" and identify the corresponding modal damping and mock shapes to enhance the performance of the notch filter and stabilize the platform motion [3].

The detailed description of the strategy, design, constraints, flight implementation and simulation of the CLKSYSID was presented in Ref. 3. This paper reviews the strategy and implementation, but focuses primarily on the results and analysis of the. in-flight CLKSYSID.

## 11. IN-FLIGHT IDENTIFICATION STRATEGY AND IMPLEMENTATION

The basic approach of CLKSYSID is to excite the stator structure using a SBA (clock actuator) torque pulse, then collect and analyze gyro data. The CLKSYSID strategy and implementation issues are reviewed first in this section to facilitate the discussion of the results and analysis in the next section.

### 2.1 The Notch Filter and inertial Mode Clock Controller Design

'l'he Galileo clock controller in inertial mode (in which gyros are used for sensing) consists of a scan commander, a proportional-integml-derivative controller, and a notch falter. It is shown in Fig. 2 with the scan commander omitted. The scan commander processes pointing commands to determine the target position of the scan platform and the slew path required to reach that position. Upon receiving the scan platform attitude information, it also generates feedback position and rate errors to feed into the controller in both clock and cone axes [5]. As mentioned before, due to the noncolocation of the sensors and actuator for the clock control loop, a wide double-notch filter was added in the loop to attenuate the control system gain at the notch frequency so that the magnitude

of the resonance peaks can be reduced to levels having reasonable stability margins. The z transfer function of the double-notch filter is

$$\frac{\text{output}(z)}{\text{input}(z)} = \left[\frac{(z - e^{-j\lambda T})(z - e^{j\lambda T})}{(z - e^{-\lambda T})^2}\right]^2$$

where $\lambda$ is the resonance frequency that is to be notched out and $T$ *is* the sampling period. The wide notch is used because of uncertainty in the knowledge of the resonance frequencies. This effectively widens the frequency range for gain attenuation. The double-notch approach provides twice the amount of attenuation as a single notch. The purpose of the in-flight identification of the stator structural resonance frequencies is to locate those "destabilizing frequencies" and the corresponding modal dampings and mode shapes so as to determine the proper parameter values for the notch filter.

## 2.2 **Spacecraft Configuration**

The spacecraft was put in inertial mode with the gyros on, The configuration showing the relationship between the stator (X, Y, Z) and plat form (M, N, 1.) coordinates is shown in Fig. 3. The scan pointing performance is measured by the pointing accuracy of the instrument bore sight vector (along the L axis). 'l"his pointing error is computed by the scan commander in terms of the position and rate error information about the platform cone N and cross-cone M axes. Motions about these two axes can be sensed by the gyros. Note that the N axis is aligned with the Y axis and that the 1., M, X, Z axes all lie on the same plane. The 1. axis may be oriented by varying the cone angle $\beta$, where $O \leq \beta \leq 2100$.

"1'here is a variation in the. observability of flexible components in the stator X and Z axes by the gyros as the cone angle $\beta$ varies. The M axis is aligned with the X axis when $\beta = 0°$, components in the X axis are completely observable and components in the. Z axis are unobservable along the M axis. For CLKSYSID, since the measurements of interest were those about the stator Z axis (excited by clock actuator about the Z axis), $\beta$ was set to 90° so that the M axis became aligned with the Z axis, Components in the Z axis became completely observable along the. M axis. Also, since the M axis is always along the gyro 1Y and 2Y axes (see Fig. 4), if a SBA torque is introduced about the Z axis, all of the flexible motion components about the Z axis are observable in the gyro 1 Y and 2Y outputs. Gyro 2Y outputs were chosen to be the primary data source for this analysis.

## 2.3 Excitation Torque

As mentioned before, SBA torque was used to excite the spacecraft flexible structure. A torque pulse. was chosen because it was easy to implement and it resembled a torque impulse. Its frequency harmonics content enabled the excitation of flexible modes over a larger frequency range of interest. However, the SBA torquer saturates at 3.8 Nm -- the software torque limiter. The only way to increase the excitation energy is to increase the torquing duration. The Power Spectrum Density (PSD) of a square pulse of width At is a function of the frequency v (in Hz), [6]

$$S(v) = \frac{\sin^2(\pi v \Delta t)}{(\pi v)^2 \Delta t} \tag{1}$$

and the nodes of the frequency harmonics are located at n/At Hz, n= 1, 2, 3, 4, . . . . Flexible modes located within about ± 0.1 Hz from each node can not be adequately excited. Therefore, it is essential to design an identification scheme, that is able to generate torques with variable pulse widths such that all the frequencies within the range of interest should be at least 0.1 Hz away from at least one node.

The l-cal-time interrupts (RTI) designed for the Galileo attitude control flight software can provide various torque pulse widths which arc multiples of 66 2/3 ms. Most of the attitude determination and control functions are executed once in this interval, Ten RTIs constitute a "minor frame" for telemetry. Five different pulses of varying widths (7, 8,9, 10 and 11 RTI) were used to ensure proper excitation of all modes within the ran ge of interest (below 15117, the gyro rolloff frequency). Two types of commands were needed to generate a torque pulse: 7S1 .EW and 7DBSE. The 7S1 .EW command was used to spin up the stator to - 10/see from rest which saturated the SBA software torque limiter (-3.8 Nm) instantly. 'I'he first 7DBSE was used to specify the desired pulse width. After a full torque excitation period, the second 7DBSE was used to lower the SBA saturation limit to the level that would just compensate the friction produced by the SBA slip ring. Thus, when the excitation was done, ideally there should be no net torque applied to the stator. Based on previous in-flight SBA friction torque calibration results, the compensation torque value was set to -0.4 Nm.

## 2.4 Telemetry Data Collection

A special mode of spacecraft telemetry, known as "flood mode" telemetry was adopted for CI .K SYSID data collection at a high sampling rate. It provides for up to six telemetry variables " every RTI (66 2/3 msec). Normally, the flood mode telemetry buffer is not part of the regular telemetry stream. To obtain the telemetry data in this mode, the buffer must be transferred to the

bulk memory in the Command Data Subsystem (CDS) once every minor frame (2/3 see) and then read out from that memory. The six telemetry channels selected were Gyro 1X, Gyro 1 Y, Gyro 2X, Gyro 2Y, SBA torque and SBA position. Each memory readout from the bulk memory contains a maximum of 38 2/3 seconds or 580 data points. As mentioned before, Gyro 2Y was the main data source for the frequency domain anal ysis.

## 2.S Gyro Data Processing

The collected raw gyro data were position measurements (O) along the M axis. However, it was the gyro rate which was used as the input to the ground software. The gyro rate (a) information was obtained by [3]

$$\omega(t_k, t_{k+1}) = \frac{\theta(t_{k+1}) - \theta(t_k)}{t_{k+1} - t_k}, \qquad \mathbf{k} = 0, \mathrm{J}, 2, \ldots$$

where $t_k$, $t_{k+1}$, $t_{k+2}$, . . . are the gyro sampled times, and ( $t_{k+1} - t_k$) is constant for all values of $k$ (66 2/3 msec, or 1 RTI) during the period the gyro samples arc collected,

## 2.6 Ground Software and identification Strategy

Two ground software programs -- CLKTDA and PAR AID were developed to analyze the gyro rate data. The first program, CLKTDA, simply generates the PSD of the gyro rate signal, The user then identifies the "peaks" in this waveform and thereby determines the. modal frequencies of the stator structure. The second program, PARAID, establishes a dynamical model of the stator structure in the clock control loop that includes all of the modal characteristics of the expected flexible modes below 151 Iz. The model consists of a transfer function of N flexible modes in the form

$$T(s) = \sum_{i=1}^{N} \frac{c_i}{s^2 + 2\zeta_i \lambda_i s + \lambda_i^2}$$

where the unknowns to be identified are: $C_i$, modal coefficients, $\zeta_i$, modal damping factors and $\lambda_i$, modal frequencies. N is number of modes with resonance frequency below the gyro rolloff frequency (15 Hz). The shape of the. PSD centered at a modal frequency is a function of the modal coefficient $c$ and damping factor $\zeta$. The relation can be easily described by considering a structural response (to a square torque pulse) to be. a damped sinusoidal function of the form,

$$f(t) = ce^{-\zeta\lambda t} \sin \lambda t$$

where A is the resonance frequency. The Fourier transform of $f(t)$ is approximately

$$g(\omega) \cong -\frac{c}{2}\left[\frac{1}{\omega - \lambda - i\zeta\lambda}\right]$$

for frequency $\omega \cong \lambda$ and $\zeta << 1$. The PSD of $f(t)$ is $|g(\omega)|^2$, which is proportional to

$$|g(\omega)|^2 \propto \frac{c^2}{(\omega - \lambda)^2 + (/j\text{-}a)'}$$

It is clear that $c^2$ affects the magnitude of $|g(\omega)|^2$ proportionally, while the magnitude (height) of $|g(\omega)|^2$ is only sensitive to the variation of $\zeta$ when the frequency is near 1. However, $|g(\omega)|^2$ becomes rather insensitive to $\zeta$ when $\omega$ moves away from $\lambda$, since $(\zeta\lambda)^2$ will become negligible compared with $(\omega - \lambda)^2$. By applying the identical excitation torque as in-flight and feeding the modal frequencies identified from CLKTDA into this model, PARAID will adjust the modal coefficient and damping, factor for each mock such that the PSD of the model output matches the PSD of the telemetry data, in frequency and amplitude, to some satisfactory accuracy. "l'he identification strategy is illustrated in Fig. 5.

## 111. RESULTS AND ANALYSIS

### 3.1 CLK SYSID Results

As mentioned in Subsection 2.3, there were five test cases corresponding to the five excitation torques with pulse widths of 7, 8, 9, 10 and 11 R']"]. The SBA excitation torque and the result ing G yro 2Y rate time histories for each case arc shown in Figs. 6-10. Per part (b) of each figure -- a close-up of the excitation torque at the RTI level, the excitation torques for each case are exactly as designed. As mentioned before, the compensation torque value after excitation was set to -0.4 Nm based on previous SBA friction torque calibration results. However, as can be seen from Figs. 6-10, this compensation torque did not cancel the average friction torque exact] y. SBA calibration on January 21, 1993 (a day after CLK SYSID) showed that average SBA friction torque was about -0.33 Nm. The effect of the residual torque is that after the excitation is done, the gyro rates gradually increase instead of holding constant, as clearly shown in Figs. 6- 10. Whether the non-constant gyro rates can cause adverse effect on the Cl .K SYSID result or not is discussed later in this section.

The first ground software program CLKTDA was then run to generate the PSDs of the Gyro 2Y rates for each case. In addition to this, the MATLAB function **spectrum.m** was also used to

generate those PSDS. The purpose of doing so is twofold. One is to double check the CLKTDA results. The other is to facilitate further analysis using MATLAB on a SUN workstation since CLKTDA is written in FORTRAN and resides on a UNIVAC mainframe. This point will become clear as we proceed. The PSDs of the Gyro 2Y rates using CLKTDA and **spectrum.m** are shown in Figs. 11-15 for the 7-11 RTJ excitation cases, respectively. The results obtained using these two programs are very similar. In general, the PSDs generated by **spectrum.m** are about an order of magnitude higher than those generated by CLKTDA. This suggested that very likely the scaling factors used in these two programs were different. However, the most important fact is that the locations of the peaks (frequencies) are the same, and the relative amplitudes between the peaks are very close. Based on these plots, peaks at 1.5, 3, 4.5 and 6 Hz were identified. The fact that these frequencies are multiples of 1.5 Hz (minor frame data rate) makes thcm suspicious as to whether they are indeed the real structural modes. Further investigation revealed that these frequencies fall right on the nodes of the PSD of the 10 RTI excitation torque square pulse (check Eq. (1)), Hence, for this 10-RTI excitation case, no mode should be excited at all at these nodes. However, they did show up in Fig. 14. Therefore, it is confirmed that these peaks are "artifact modes", not real structure modes.

### 3.2 **Analysis Through Simulation**

To investigate where these artifact modes came from and why no structural modes were evident, a simple dynamic model (Fig. 16) consisting of the rigid body as well as two flexible modes and a gyro model (Fig. 17) was developed and a series of simulations were conducted using SIMULINK. The flexible modes selected were the two dominant modes used in the simulations in Ref. 3. They were the dominant modes in an older version of the ground mock]. However, for this simulation, the modal damping $\zeta$ was set to 0.25% for both modes instead of 0.34% and 0.23% as in Ref. 3. To summarize, the modal characteristics of these two modes are:

| Modal Frequency $\lambda_i$ / 271 (Hz) | Modal Coefficient c, | Modal Damping $\zeta_i$, % |
|---|---|---|
| 8.43 | -6.594 x 10-3 | 0.25 |
| 9.31 | --5.966 x 10-3 | 0.25 |

The Bode magnitude plot of the system is shown in Fig. 18. The two peaks confirm that the dominant modes arc indeed located at 8.43 ant] 9.311 Iz. The same 10 RTISBA excitation torque was injected into the system with a 0.05 Nm residual torque following the completion of the excitation, as shown in Fig. 19. The gyro position data were then collected and processed to generate gyro rate in exactly the same way the flight data were processed. The simulated gyro

position and rate time histories are shown in Fig. 20. Comparing Fig. 9(c) and Fig. 20(b), it can be seen how close the real and the simulated gyro rates arc for the 10 RTI excitation case, indicating that the imperfect compensation of SBA friction torque was truthfully emulated. MATLAB function **spectrum.m** was then used to generate the PSD of the resulting gyro rates, as shown in Fig. 21. The two modes excited *were* at about 5.7 Hz and 6.6 Hz, the aliased modes of the 9,31 Hz and 8.43 Hz modes seeded in the model (about the Nyquist Frequency 7.5 Hz, half of the sampling rate). It is interesting to note that no artifact modes were observed, revealing that the imperfect compensation of the SBA friction (thus the non-constant gyro rate after the excitation) had nothing to do with the artifact modes.

It was hypothesized that the most possible cause of the artifact modes was the I/O timing error. The gyro data appearing in the telemetry were the gyro position data. Ideally every 10 RTI (1 minor frame, 2/3 see) CDS reads the last 10 data points into CDS memory, then commands are issued to read out the CDS memory. I lowever, the timing of this process on-board may not be perfect. If CDS reads the data a little earlier or a little later than exactly one minor frame, it will result in errors when the gyro rate is calculated by the ground software, and an artifact effect may occur. To emulate this situation, 6 micro radians was added to the gyro position data at RTI 1 of the minor franc and subtracted out at RTI2. A random number generator and an index were used to control the probability with which the above-mentioned imperfect timing occurs. 'l'he probability was varied from 30%, 5070, 70% to 100% in the simulations. For each case, PSDs of the gyro rates were generated using **spectrum. m** and plotted in Fig. 2.2. It can be seem that as the probability of imperfect timing increases, the artifact modes of 1.5 Hz, 3 Hz, 4.5117. and 6 Hz become more and more evident. The important finding, however, is that the real modes are essentially unaffected as compared with those in Fig. 21, Hence, it is concluded that if any flexible modes were excited by the applied SBA torque, they would not be "buried" due to the existence of artifact mocks.

Since the Low Gain Antenna (LGA) swing test for the High Gain Antenna (HGA) anomaly investigation found that the damping of the spacecraft's flexible modes was much higher than expected (some of them as high as 2%) [7], another simulation was run by setting the damping of the two dominant modes in the SIMULINK model to 2% with no artifact effect. The resulting gyro rate PSD is shown in Fig. 23. The two modes almost disappeared as compared with those in Fig. 21 (0.25% damping). By repotting Fig. 14(b) (the in-flight 10 RTI excitation case) using the same scale of Figs. 21 -23 and omitting the artifact modes, the resulting plot (Fig. 24) is extremely close to that of the 2% damping case (Fig. 23). Comparing with the two modes in Fig. 21, they are both clearly in the noise level. This indicates that higher damping could very possibly be the cause

of the absence of true modes on the PSD plots. Since no significant modes were identified, it was not necessary to run the second ground software PARAID.

## IV. CONCLUSIONS

After Galileo's flight data was processed using the CLK SYSID ground software, no prominent stator flexible modes were identified, Artifact modes with frequencies at multiples of 1.5 Hz (minor frame data rate) showed up instead. Simulations demonstrated that these artifact modes could possibly be due to on-board data I/O timing error. The leading explanation for the absence of any true structural modes is that the damping of the flexible modes was higher than expected, and therefore, true stator modes simply could not be excited by the torques applied. In any event, the flexibility of the stator presents no adverse effect to the stability and performance of the clock controller, thus none of the clock controller parameters need to be updated.

## ACKNOWLEDGEMENTS

The research described in this paper was carried out at the Jet Propulsion Laboratory, California institute of Technology, under contract with the National Aeronautics and Space Administration.

## REFERENCES

[1] McGlinchey, L. F., "Planetary Spacecraft Pointing and Control -- The Next 20 Years," American Astronautical Society, A AS Paper 80-017, February 1980.

*[2]* Rasmussen, R. D. and T. K. Brown, "Attitude and Articulation Control Solutions for Project Galileo," American Astronautical Society, AAS Paper 80-109, February, 1980.

[3] Wong, E. C., "In-Flight Identification of the Galileo Spacecraft Flexible Mode Characteristics," AIAA Journal of Guidance, Control and Dynamics, Vol. 9, No. 1, January - February, 1986.

*[4]* Macala, G., "Galileo S/C Clock Controller Redesign for Operation in the 66 2/3 msec Rate Group," JPL internal memo EM 343-789, February 28, 1983.

*[s]* Chodas, J. L. and G. K. Man, "Design of the Galileo Scan Platform Control," Journal of Guidance, Control and Dynamics, Vol. 7, p. 422, July - August, 1984.

[6] Papoulis, A., "Probability, Random Variables and Stochastic Processes," McGraw-Hill Book Co., Ncw York, 1965.

[7 Singh, G., "Galileo LGA-2 Retraction Results: Dynamics Assessment", JPL internal memo IOM 343-92-636, December 3, 1992.

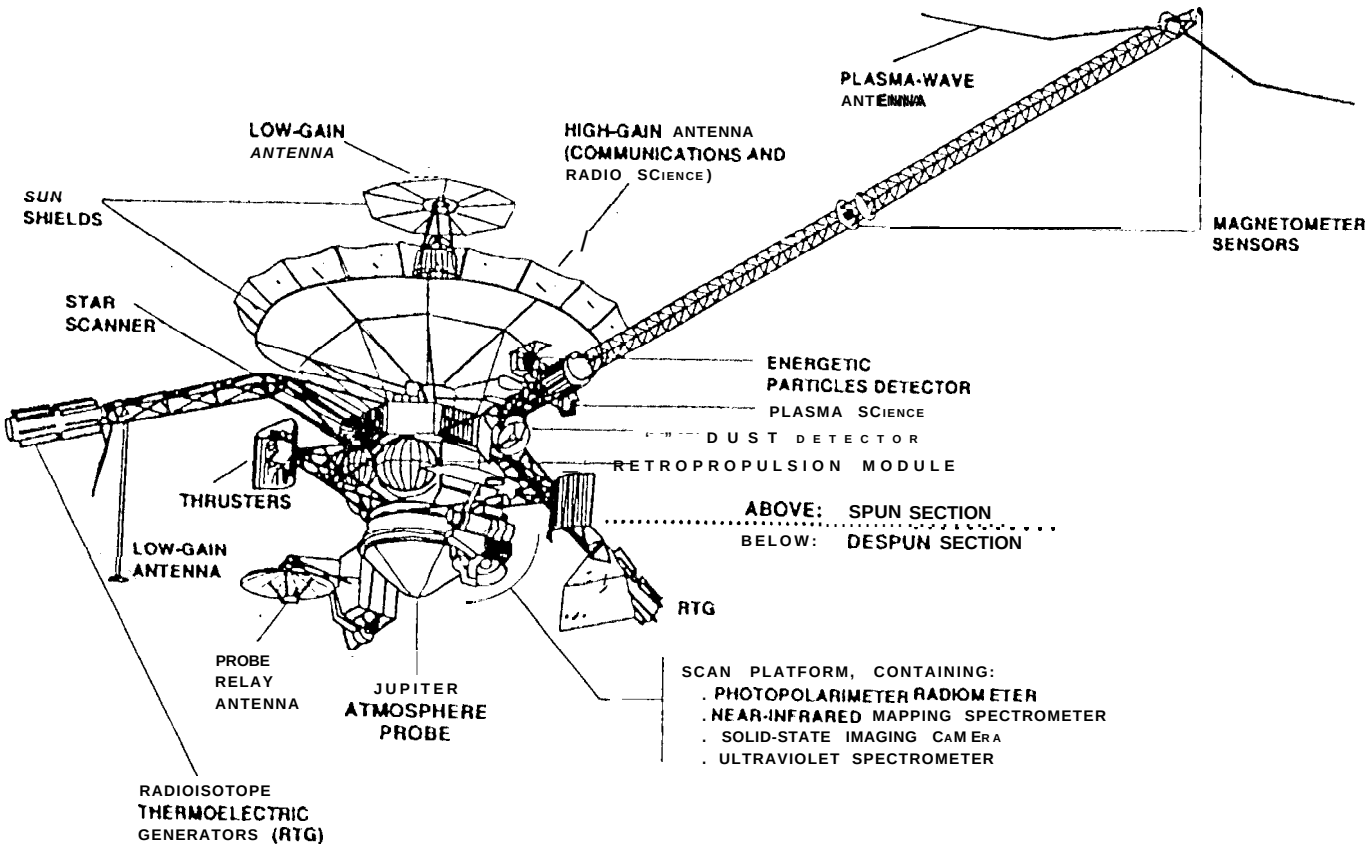


Figure 1. Galileo Spacecraft

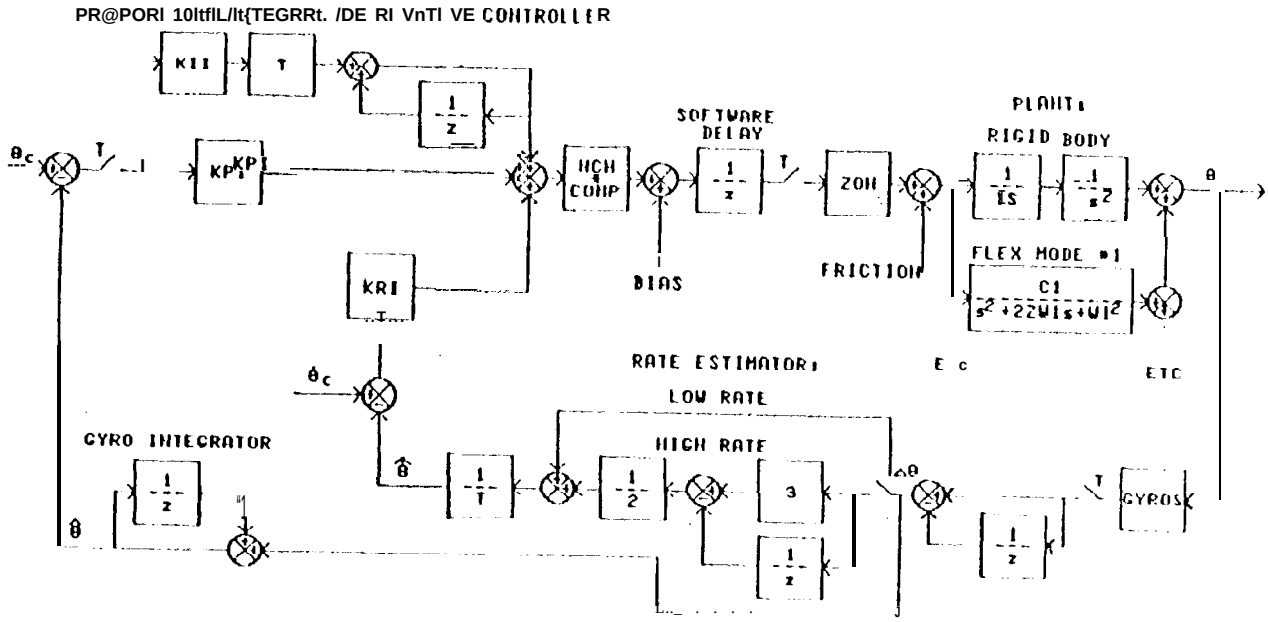


Figure 2. Clock Inertial PID Controller

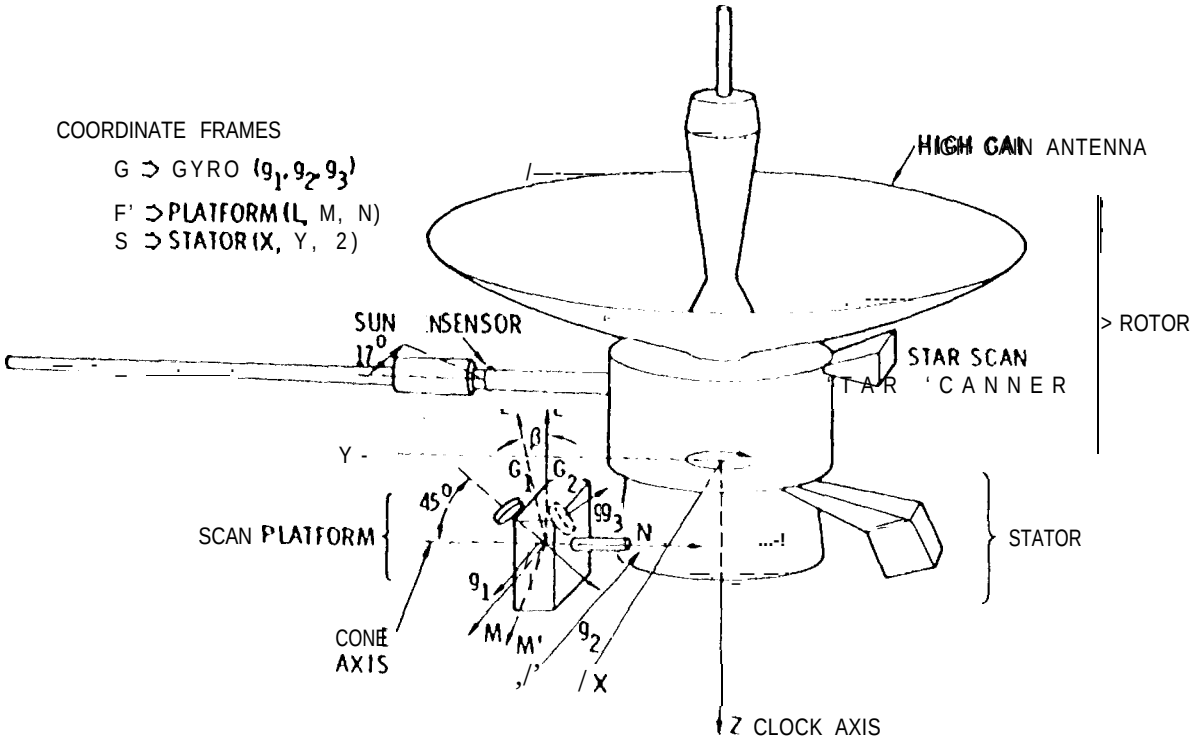


Figure 3. Galileo Spacecraft Stator and Platform Coordinate S ystems

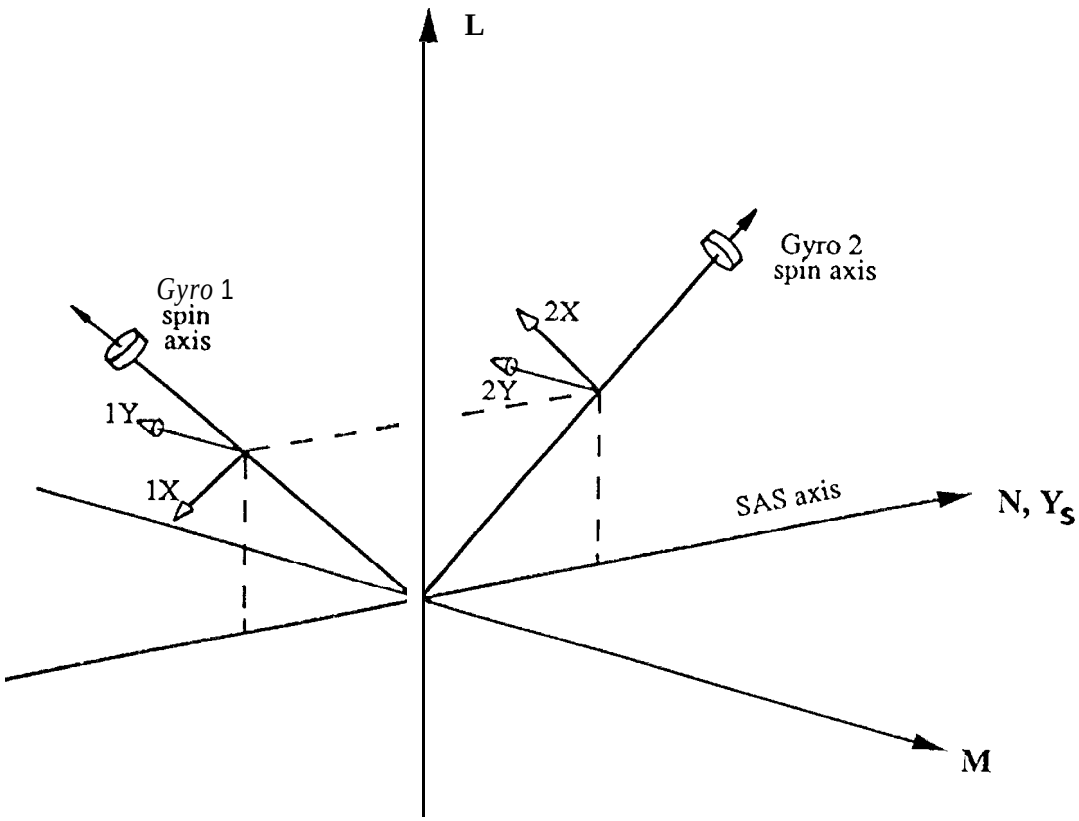


Figure 4. Scan Platform and Gyro Axes

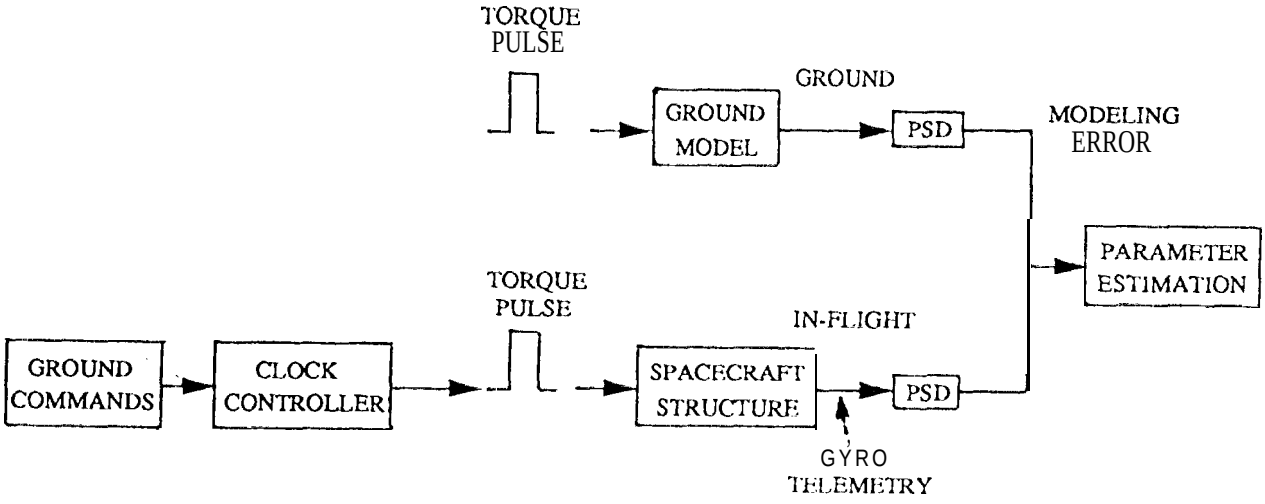


Figure 5. Clock System Identification Strategy

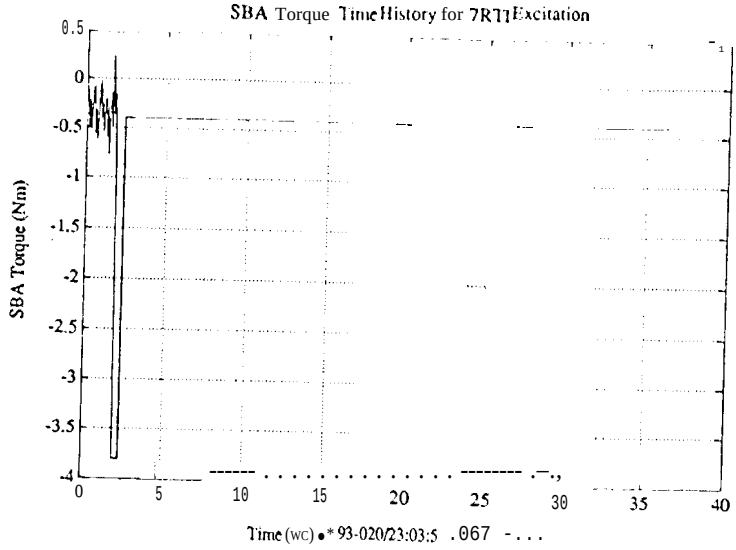


(a) Excitation Torque

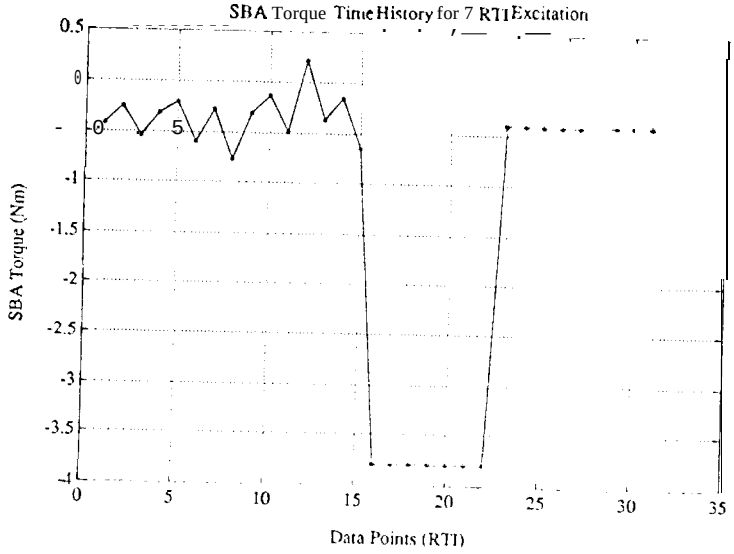


(b) Close-Up of Excitation Torque

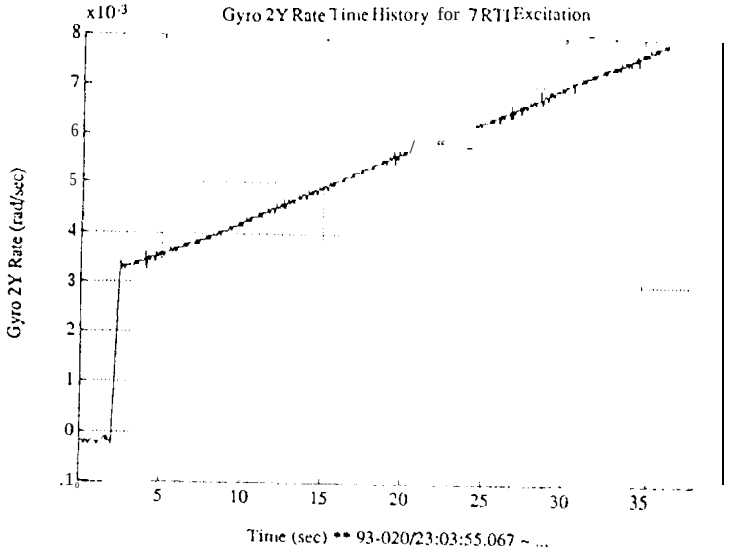


(c) Gyro 2YRate

Figure 6. 7 RTI SBA Excitation Torque and Gyro 2Y Rate Time Histories

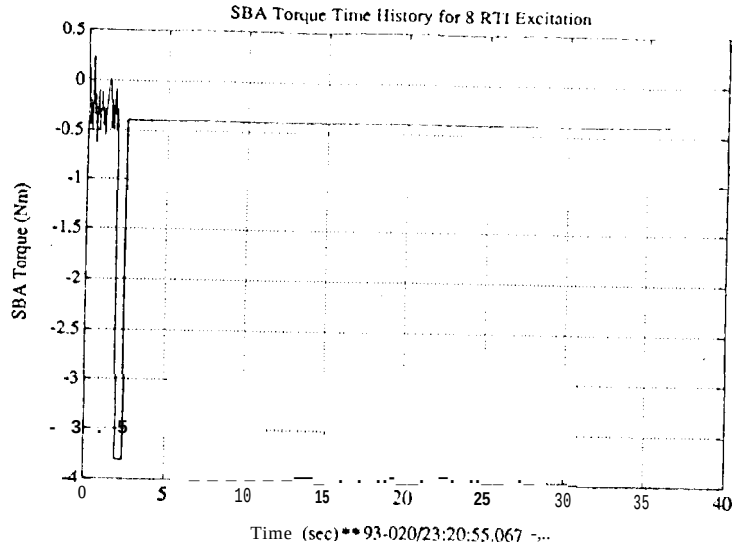


(a) Excitation Torque

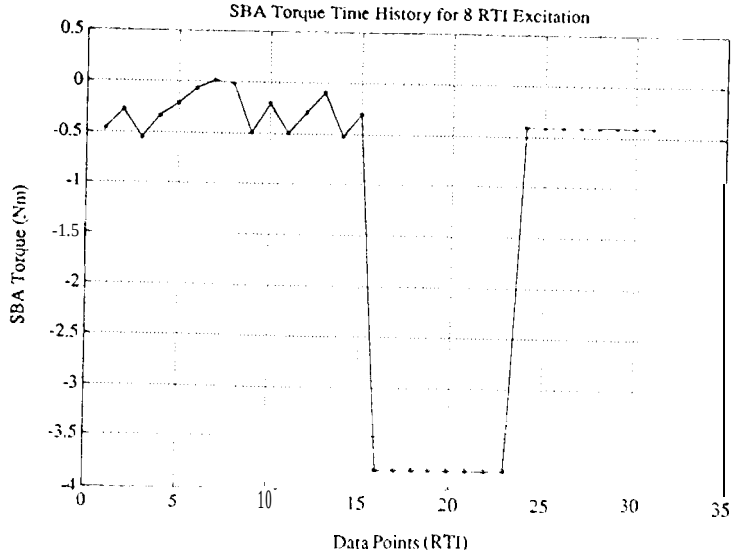


(b) Close-Up of Excitation Torque

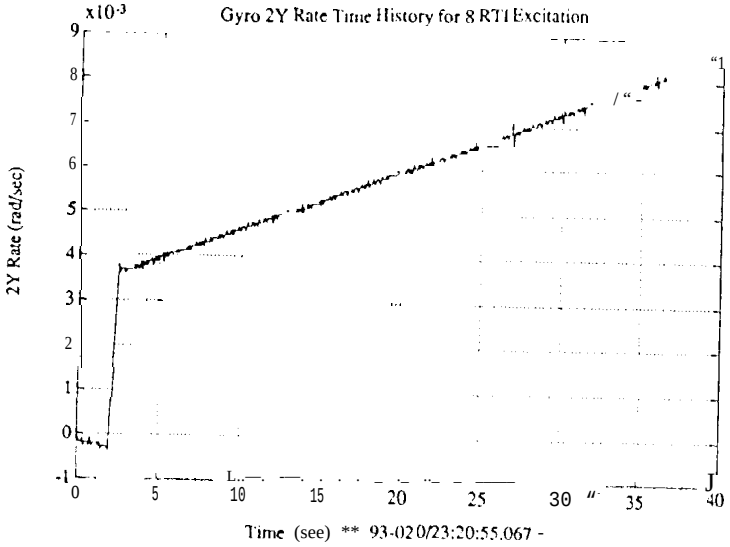


(c) Gyro 2Y Rate

Figure 7. 8 RTI SBA Excitation Torque and Gyro 2Y Rate Time Histories

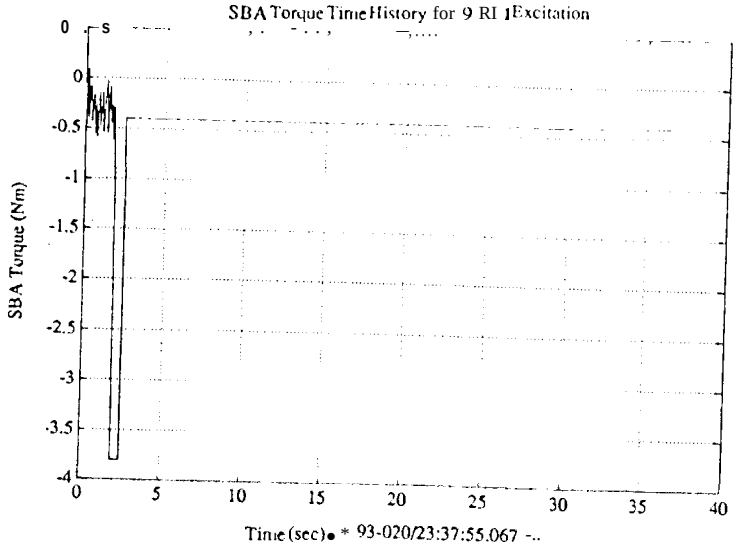


(a) Excitation Torque

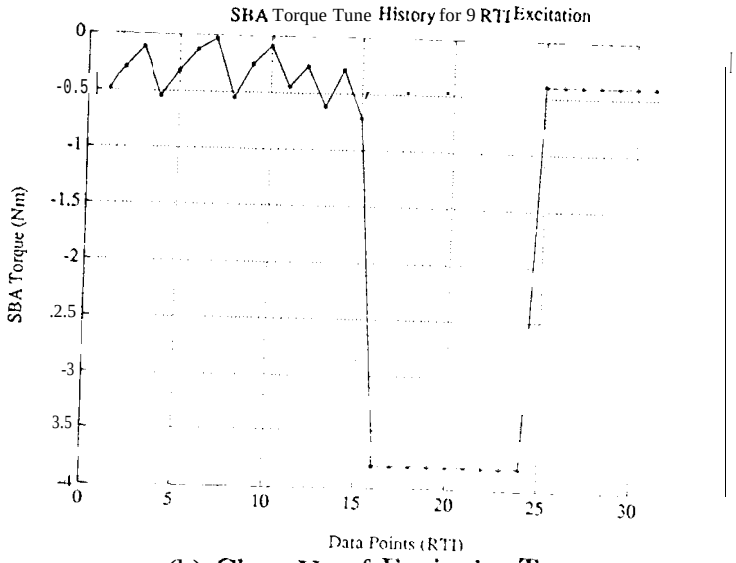


(b) Close-Up of Excitation Torque

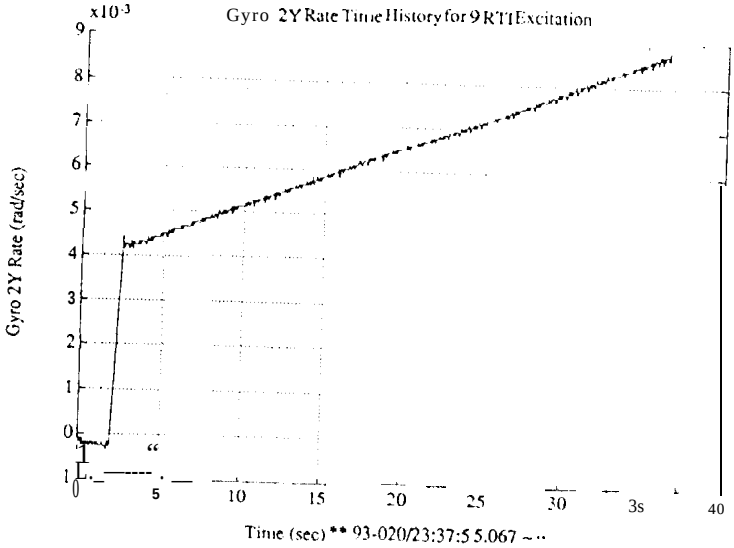


(c) Gyro 2Y Rate

Figure 8. 9 RTI SBA Excitation Torque and Gyro 2Y Rate Time Histories

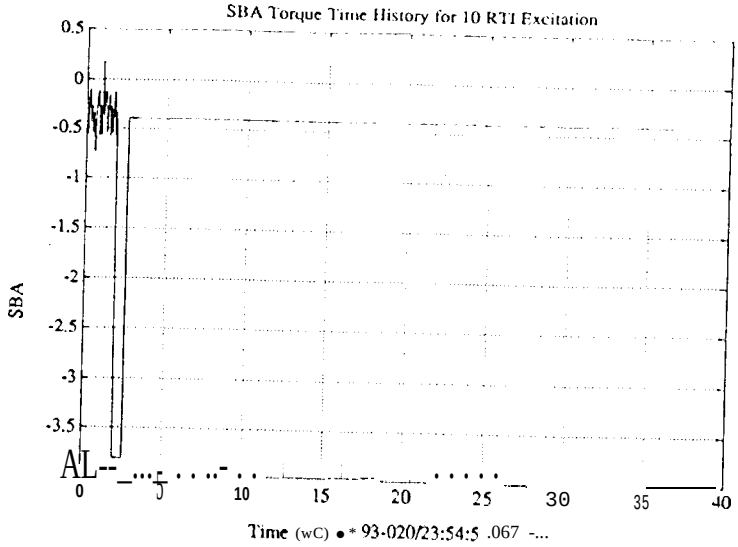


(a) Excitation Torque

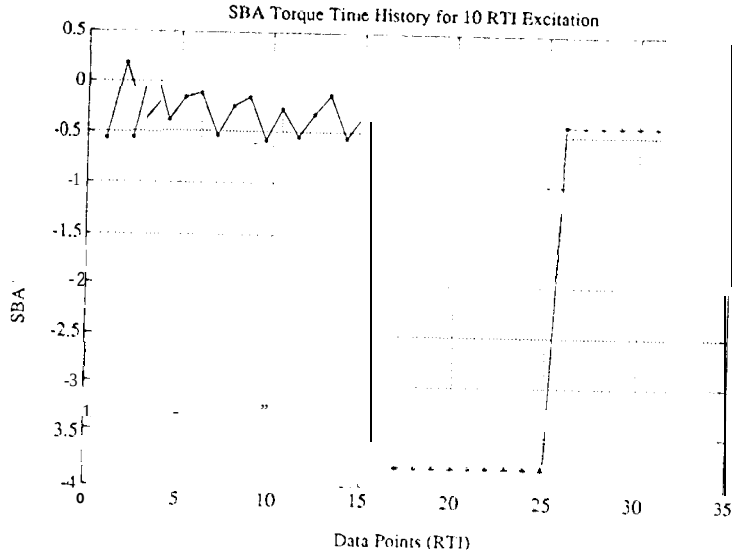


(b) Close-Up of Excitation Torque

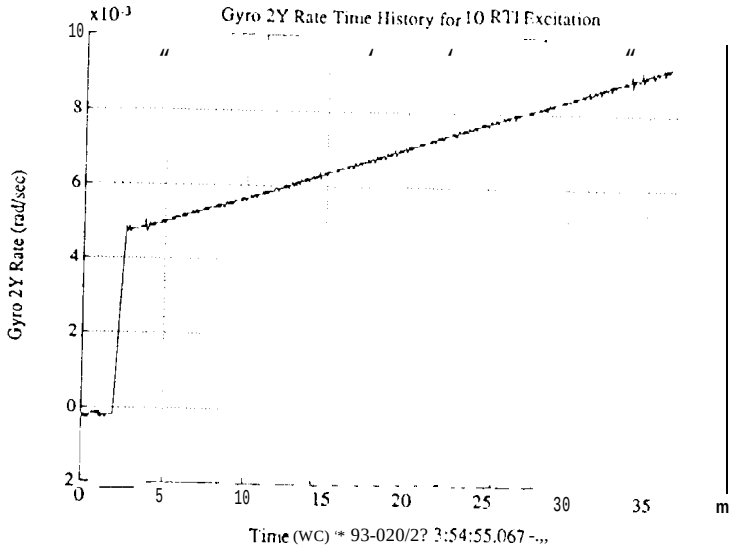


(C) Gyro 2Y Rate

Figure 9.10 RTI SBA Excitation Torque and Gyro 2Y Rate Time Histories

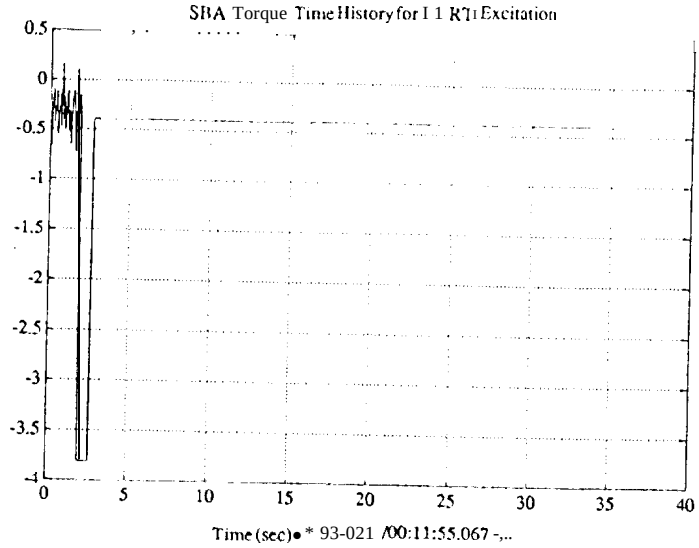


(a) Excitation Torque

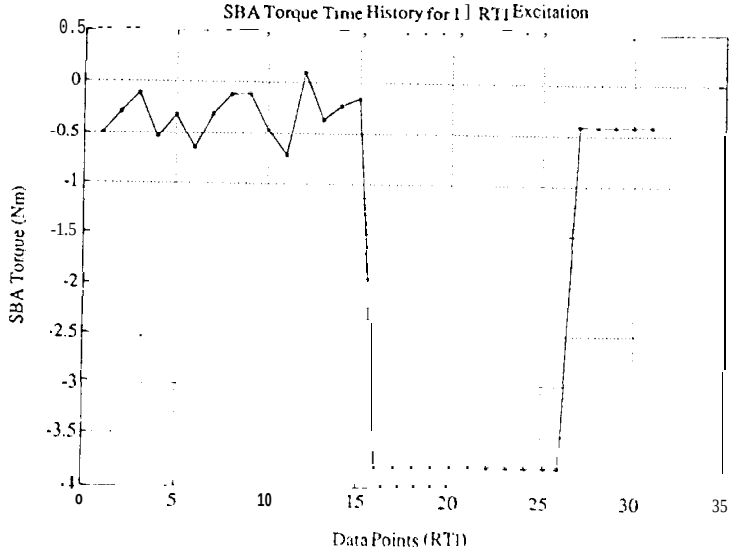


(b) Close-Up of Excitation Torque

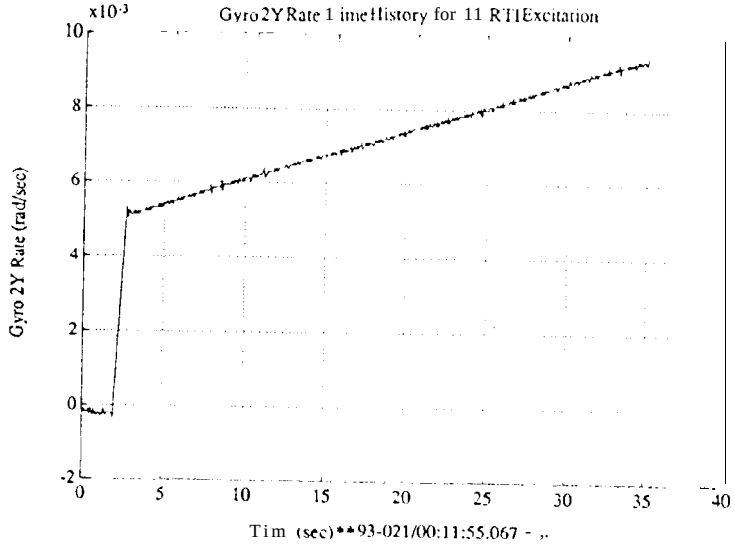


*(c) Gyro 2Y* Rate

Figure 10. 11 RTI SBA Excitation Torque and Gyro 2Y Rate Time Histories

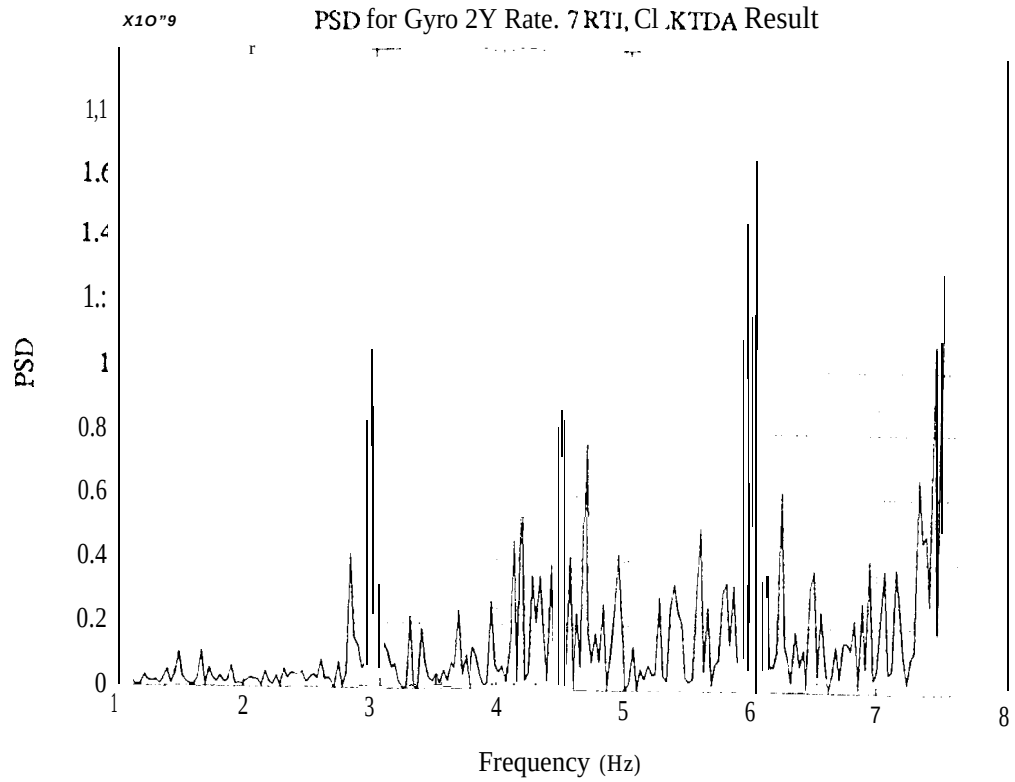


(a) Ground Software CLKTDA Result

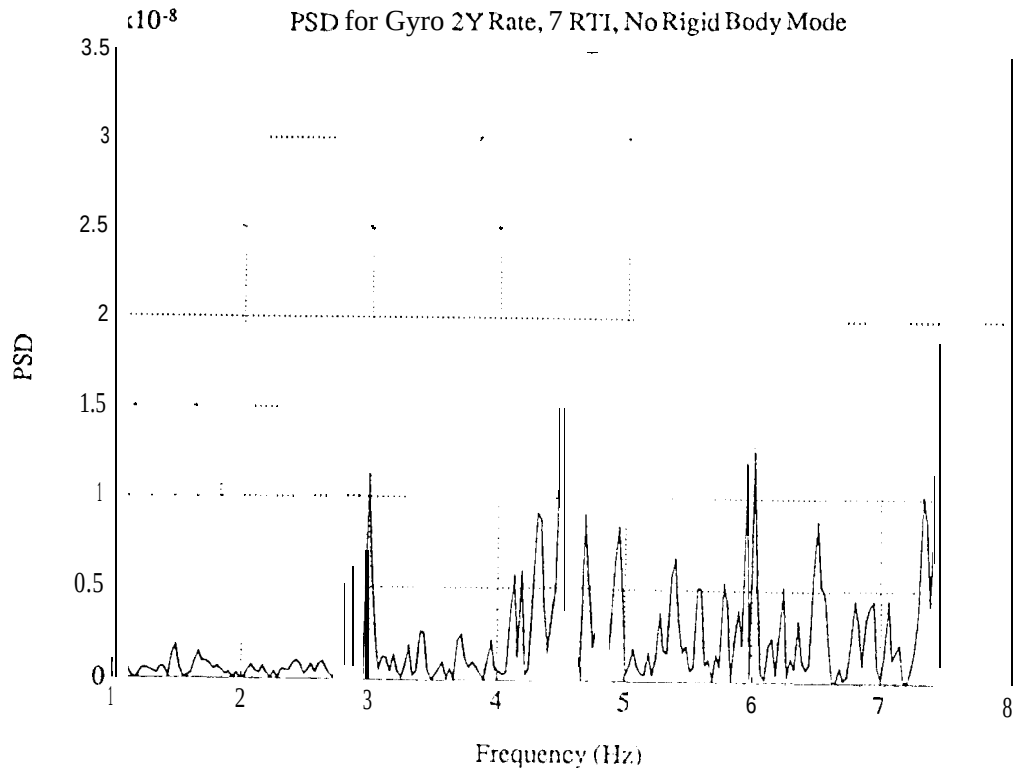


(b) MATLAB Function spectrum.m Result

Figure 11. PSD of Gyro 2Y Rate for the 7 RTI Excitation Case

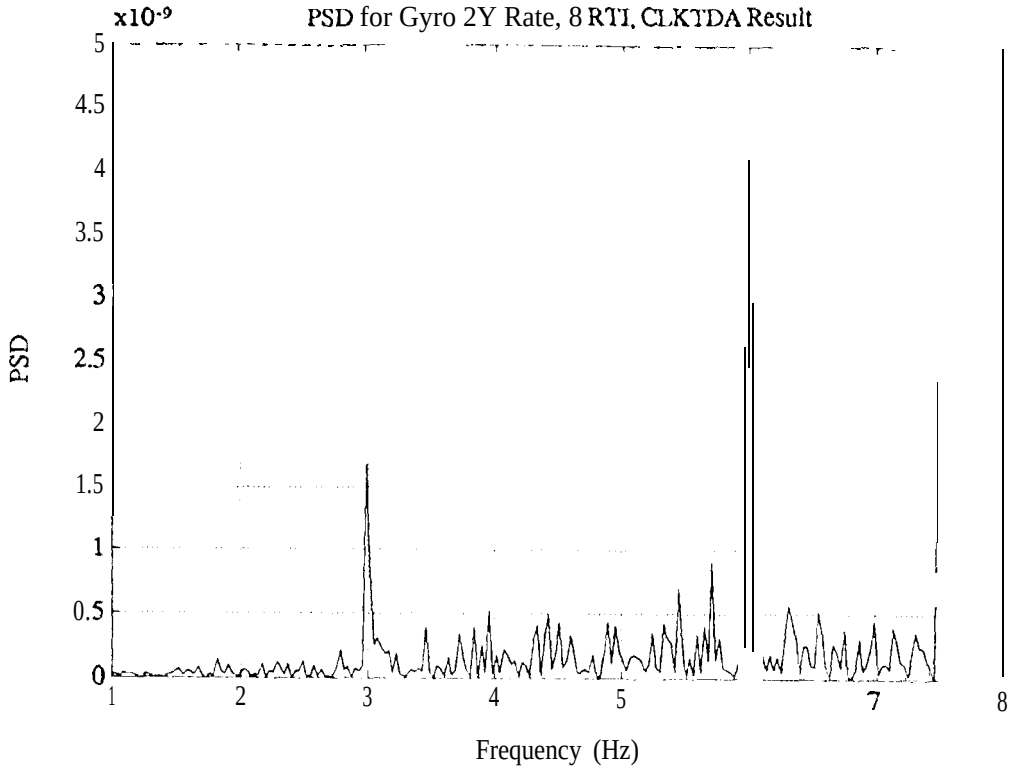


(a) Ground Software CLKTDA Result

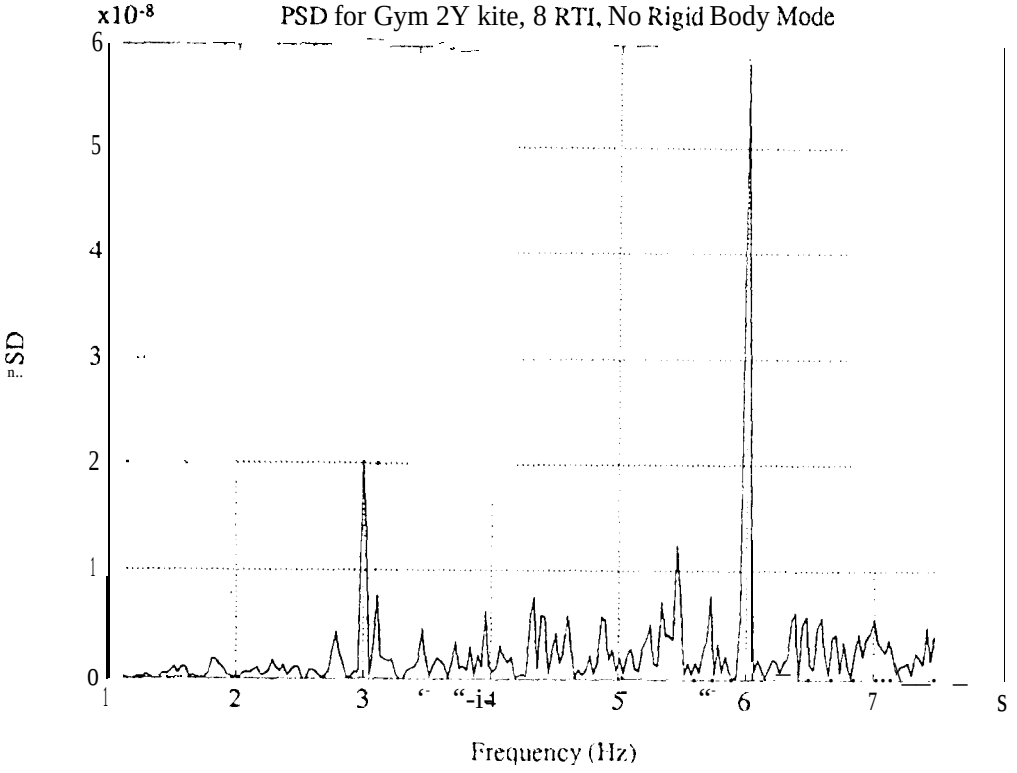


(b) MATLAB Function **spectrum.m Result**

Figure 12. PSD of Gyro 2Y Rate for the 8 RTI Excitation Case

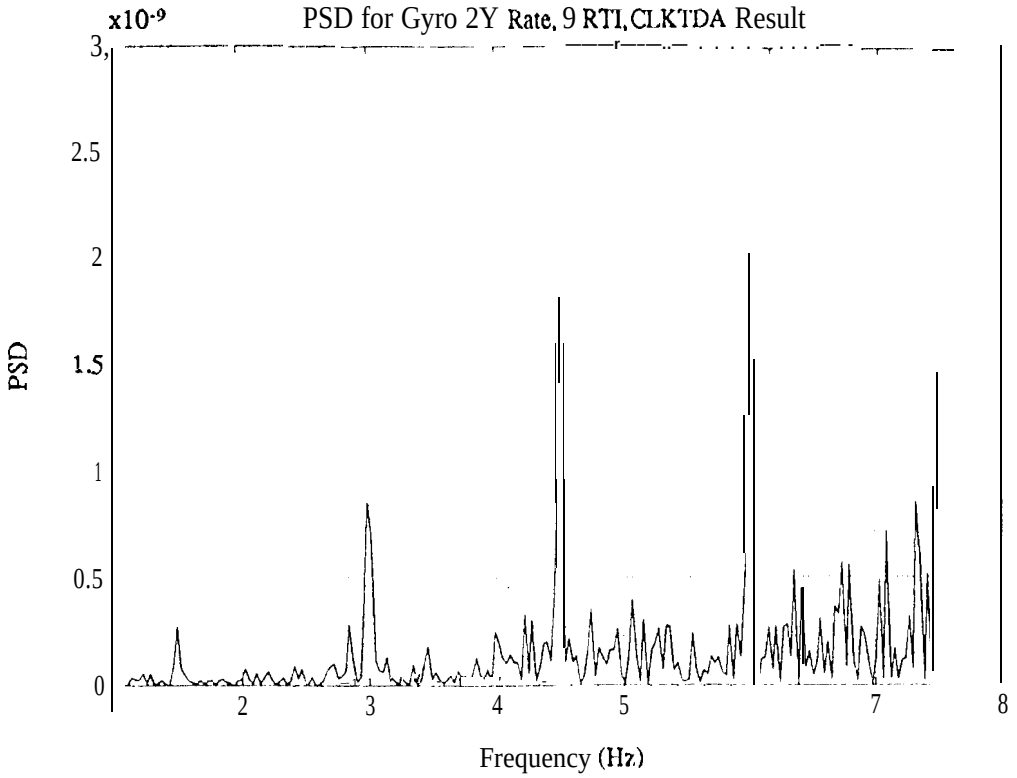


(a) Ground Software CLKTDA Result

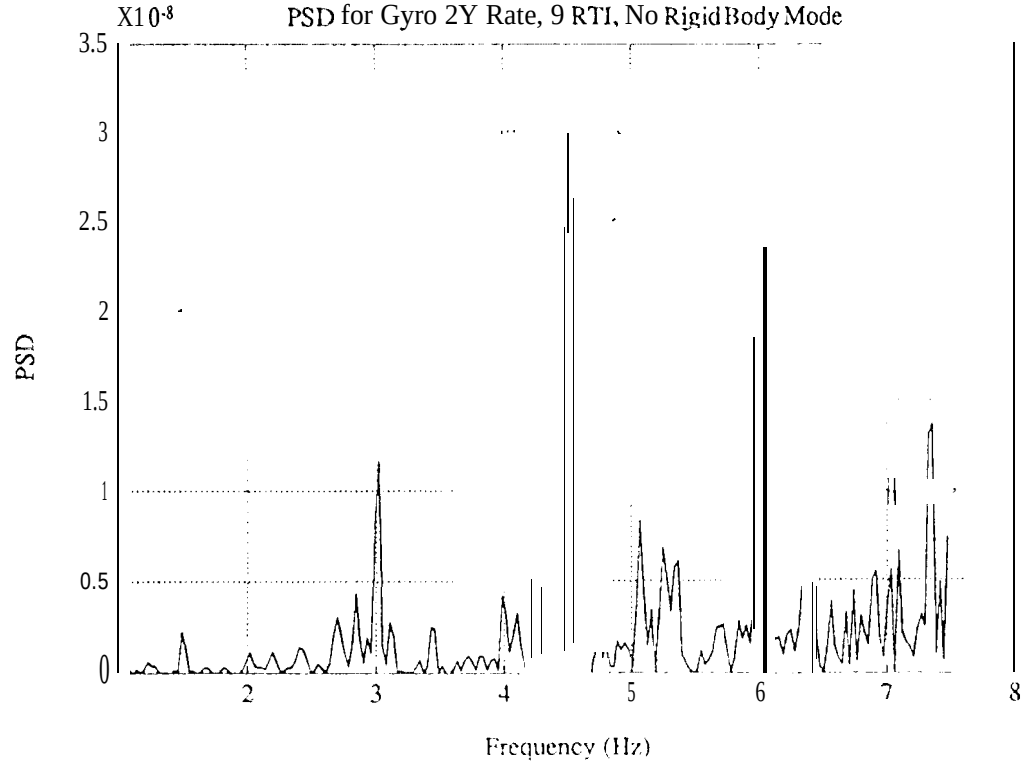


(b) MATLAB Function **spectrum.m** Result

Figure 13. PSD of Gyro 2Y Rate for the 9 RTI Excitation Case

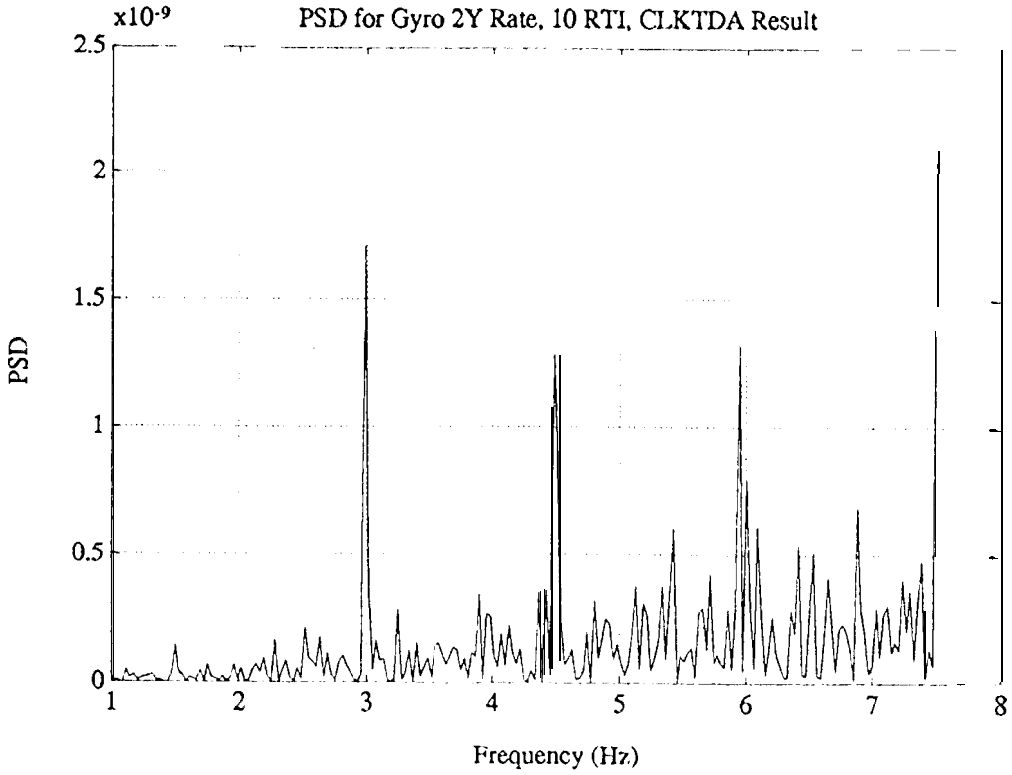


(a) Ground Software CLKTDA Result

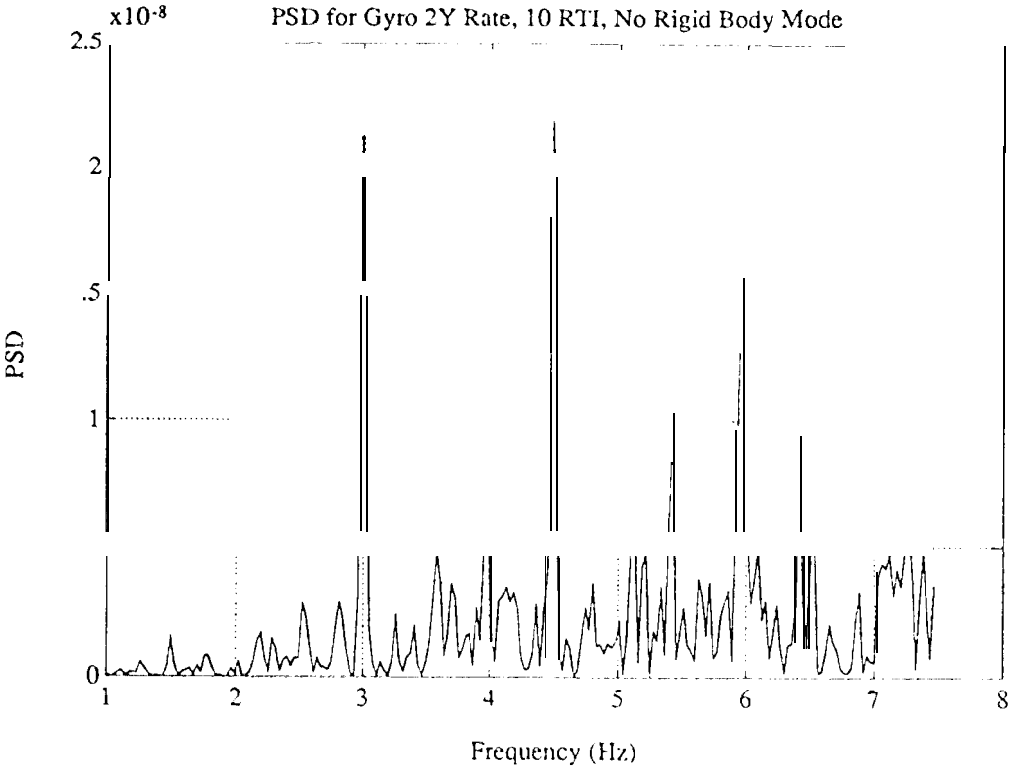


(b) MATLAB Function **spectrum.m** Result

Figure 14. PSD of Gyro 2Y Rate for the 10 RTI Excitation Case

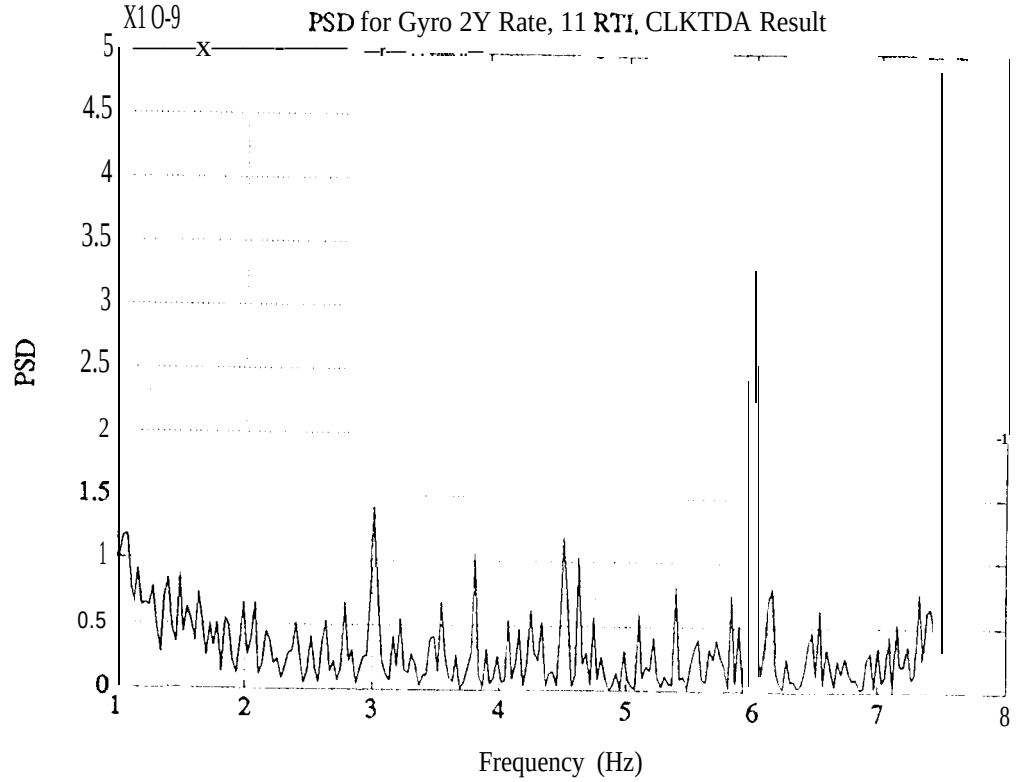


(a) Ground Software CLKTDA Result

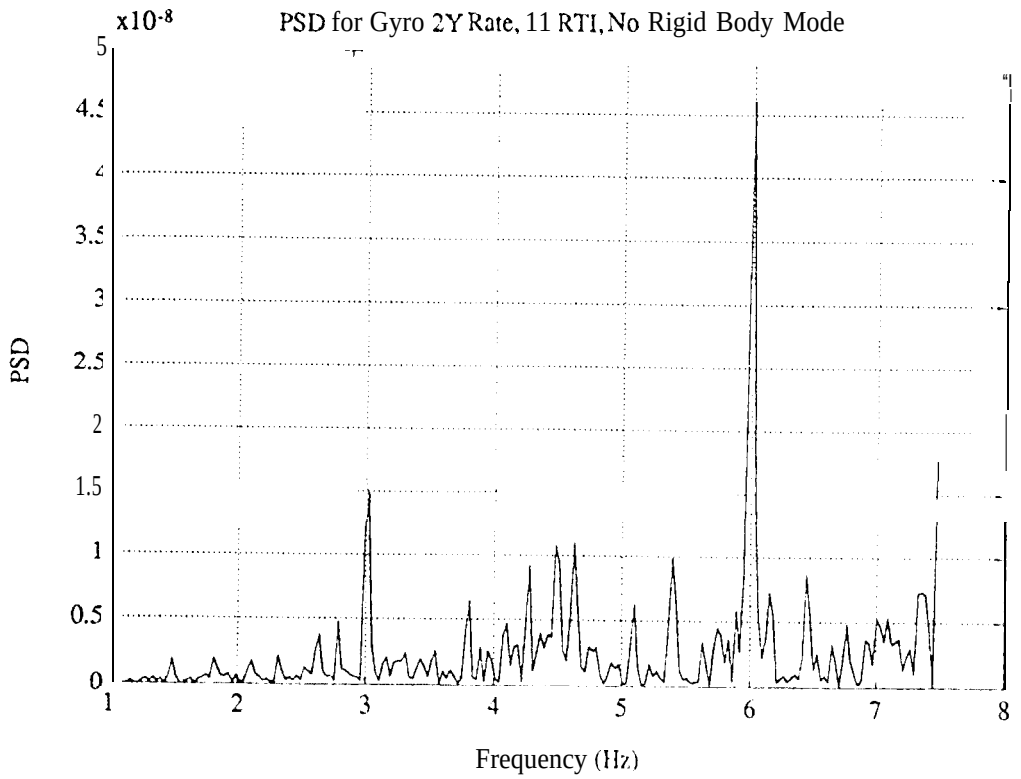


(b) MATLAB Function **spectrum.m** Result

Figure 15. PSD of Gyro 2Y Rate for the 11RTI Excitation Case

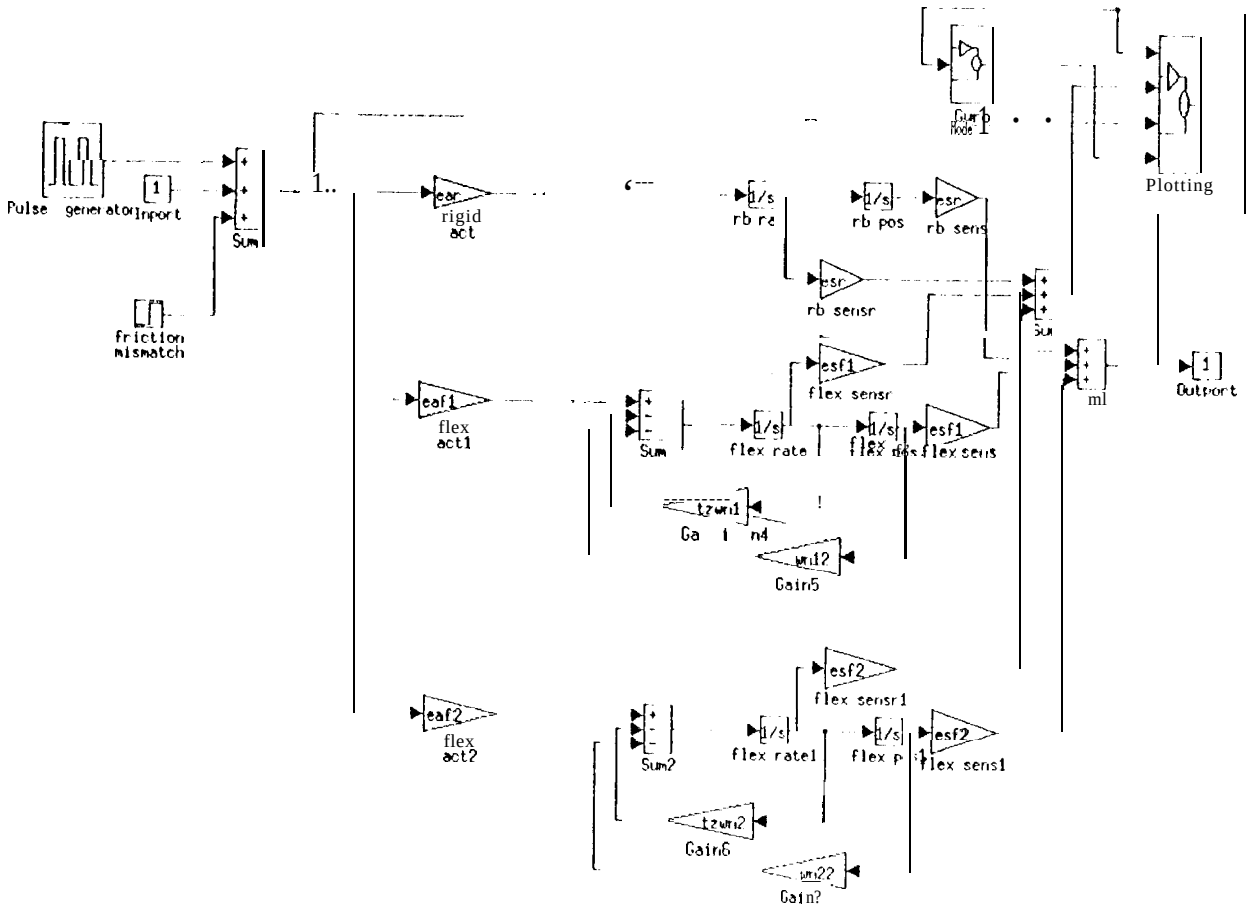


Figure 16. SIMULINK Dynamic Model for the Investigation of the CLK SYSID Artifact Modes

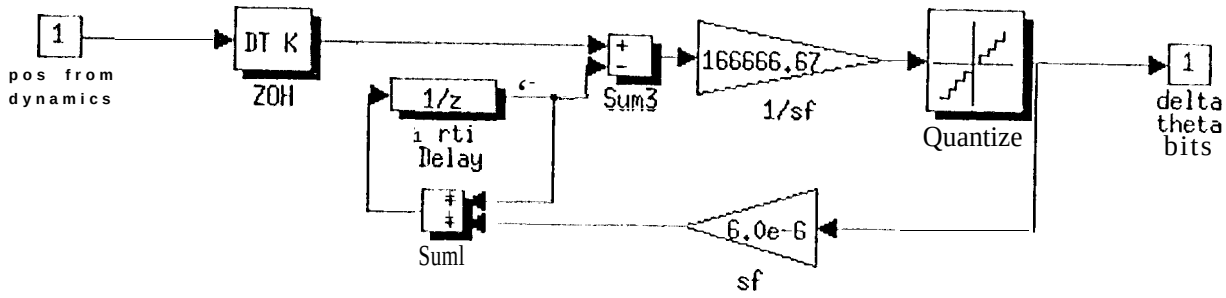


Figure 17. The Gyro Model

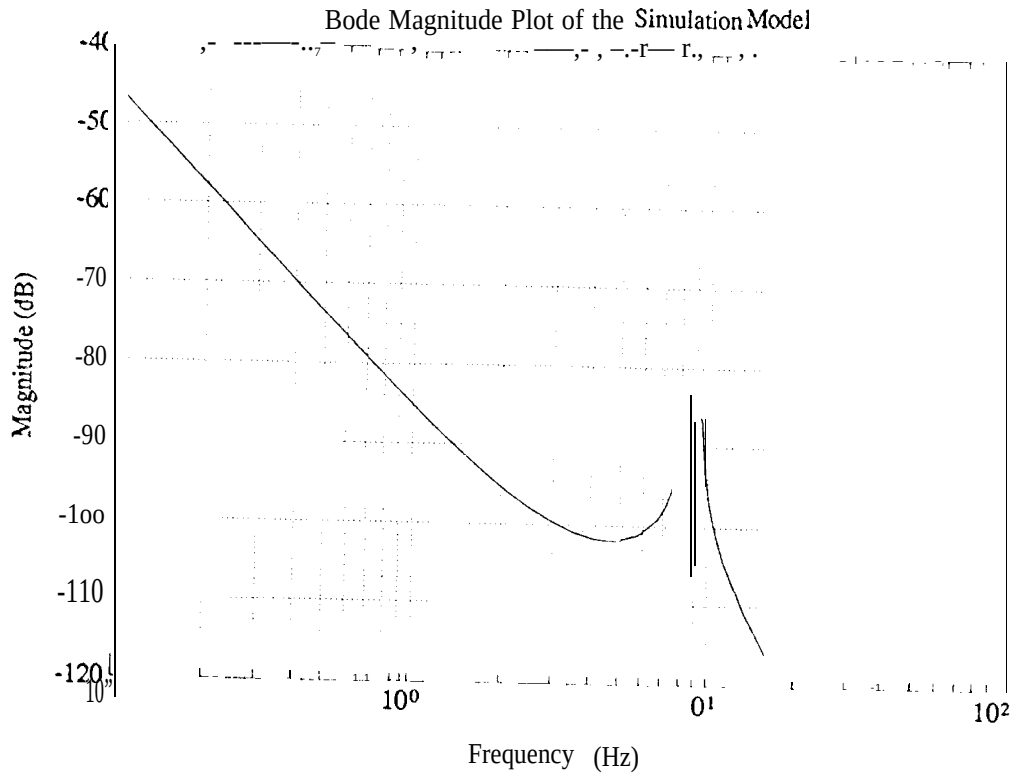


Figure 18. Bode Magnitude Plot of the SIMULINK Model

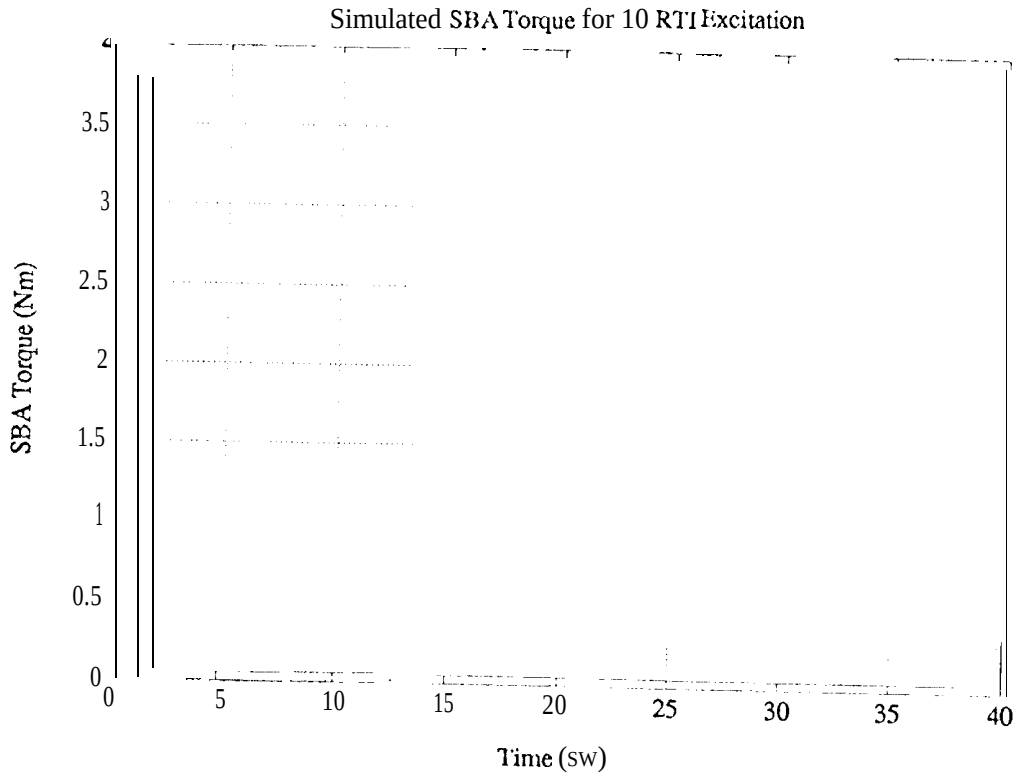


(a) Simulated Recitation Torque

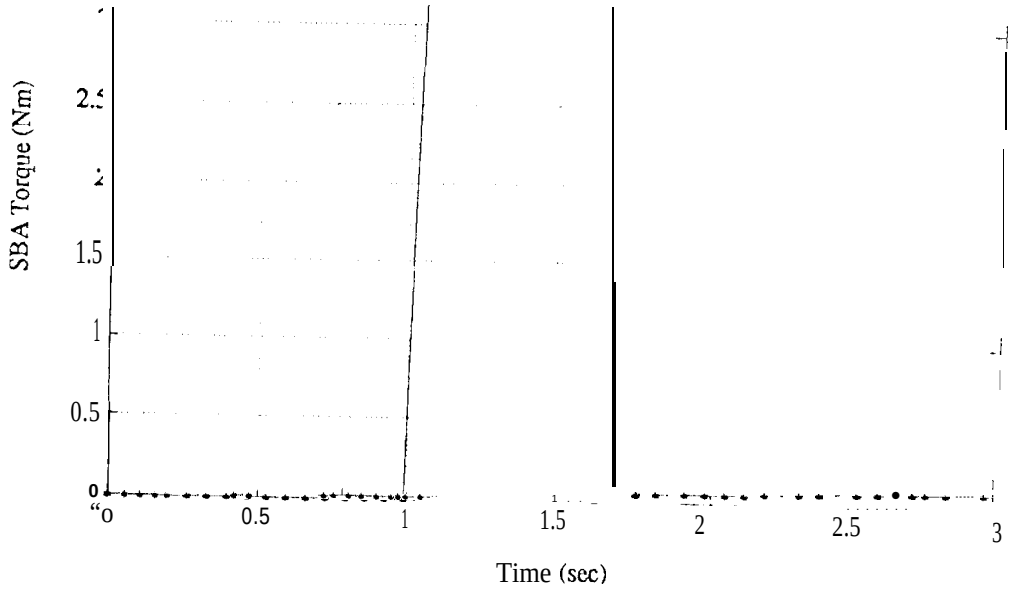


(b) Close-Up of the Simulated Excitation Torque

Figure 19. Simulated 10 RTI SBA Excitation Torque (SIMULINK Results)

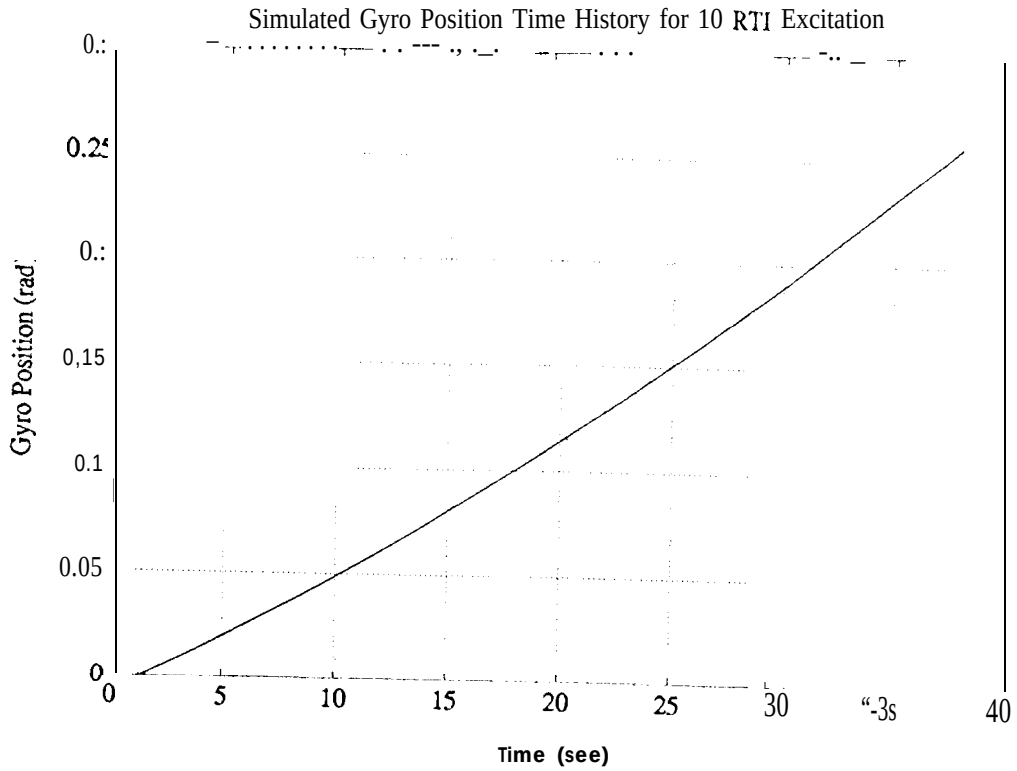


(a) Simulated Gyro Position

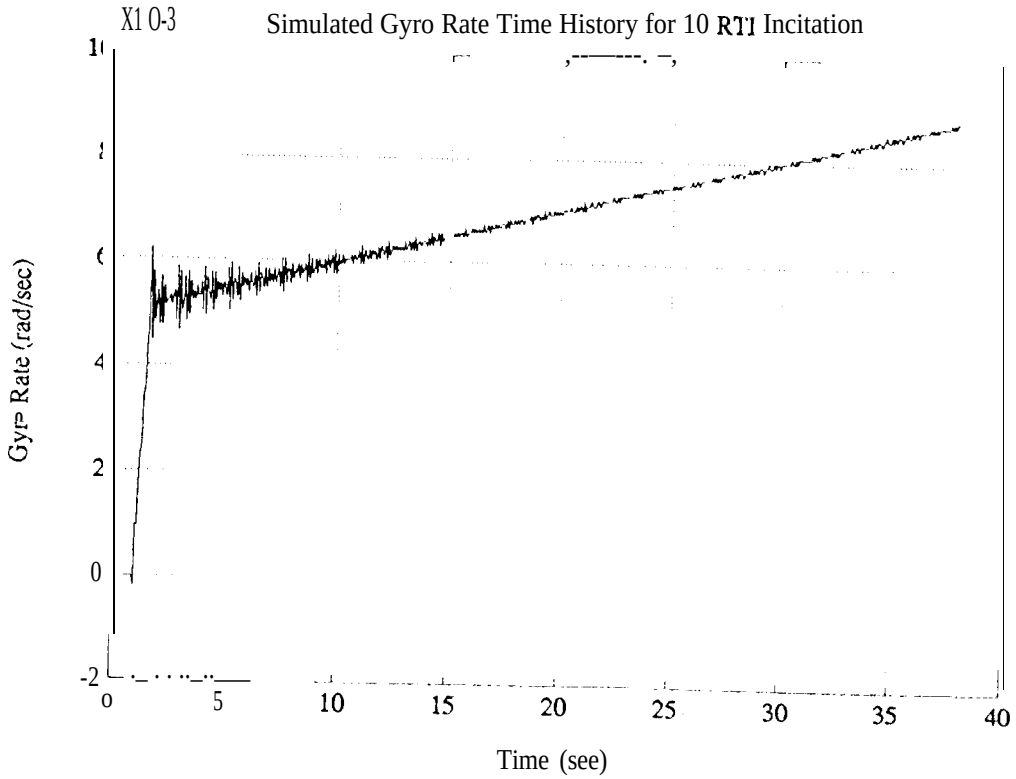


(b) Simulated Gyro Rate

Figure 20. Simulated Gyro Position and Rate for 10 RTI Excitation (SIMULINK Results)

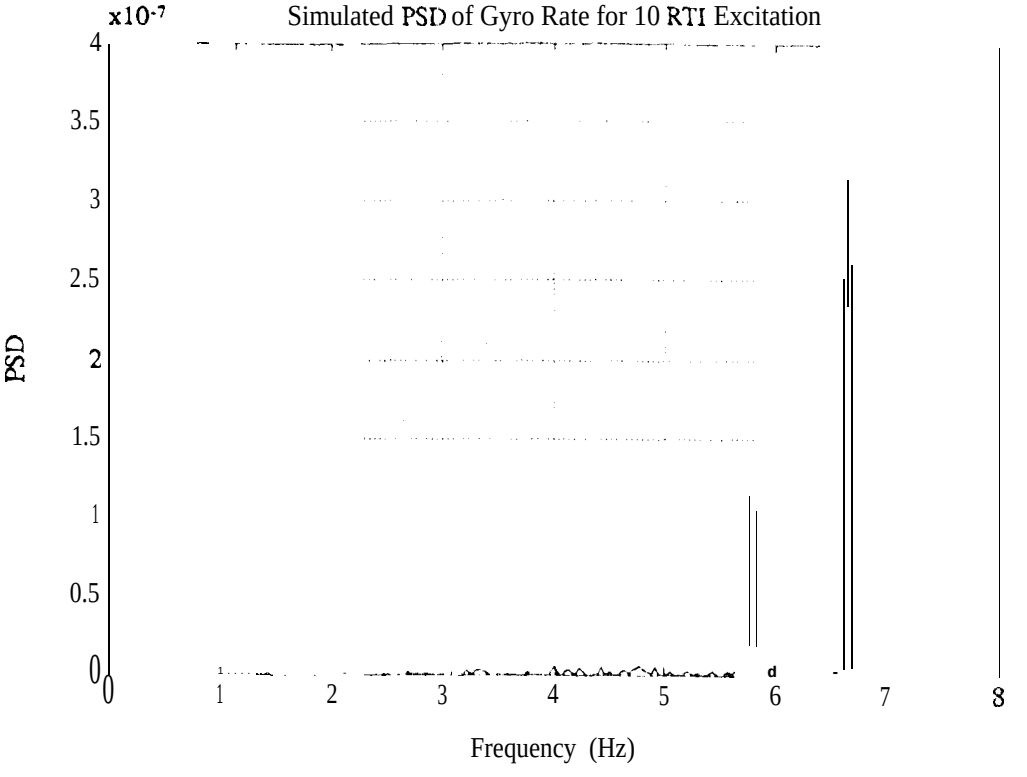


Figure 21. Simulated PSD of Gyro Rate for 10 RTI Excitation (SIMULINK Results)

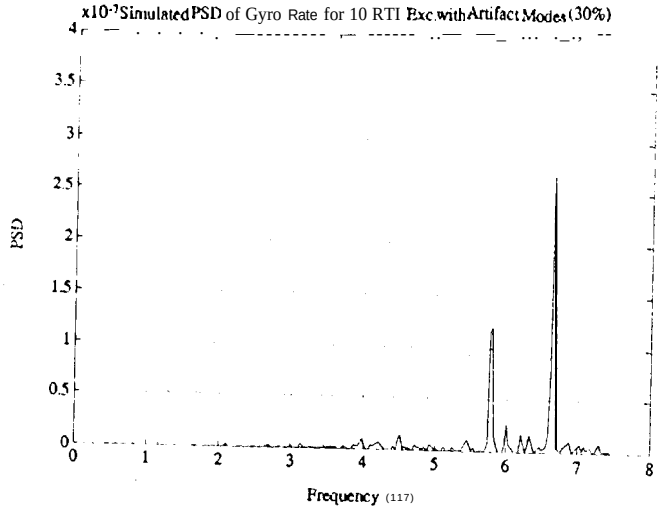


(a) 30% Probability of Imperfect Timing

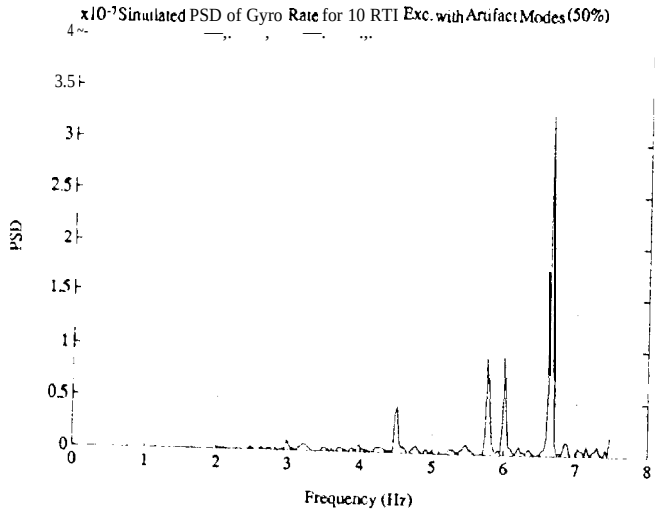


(b) 50% Probability of imperfect Timing

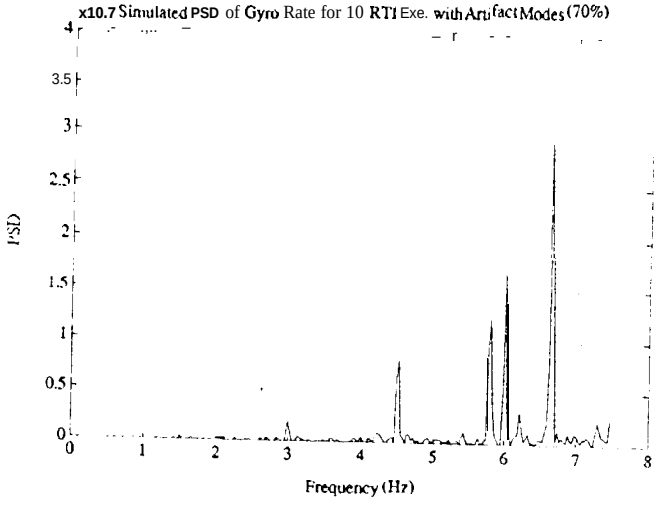


(c) 70% Probability of Imperfect Timing

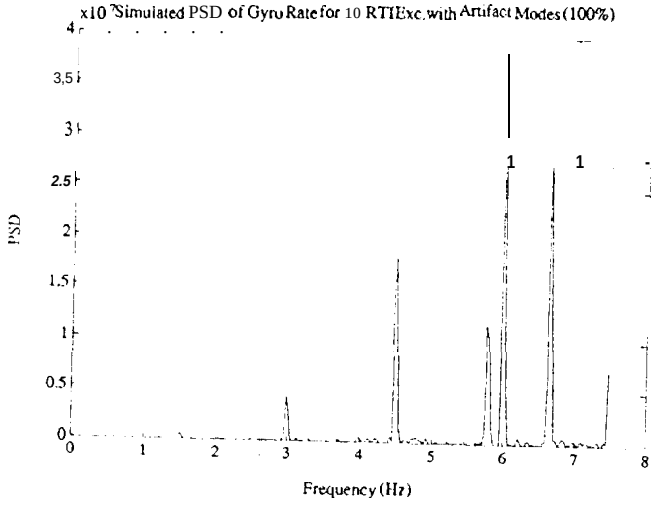


(d) 100% Probability of Imperfect Timing

Figure 22. Simulated PSD of Gyro Rate for 10 RTI Excitation with imperfect Timing Effect (SIMULINK Results)

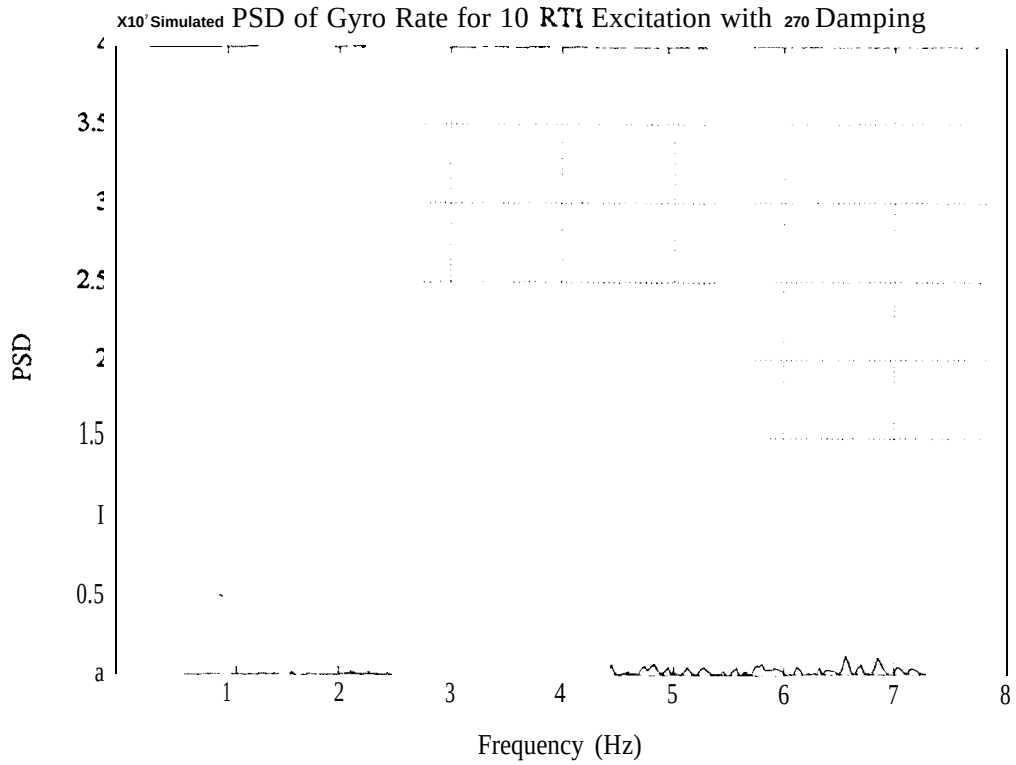


Figure 23. Simulated PSD of Gyro Rate for 10 RTI Excitation with 2% Damping (SIMULINK Results)

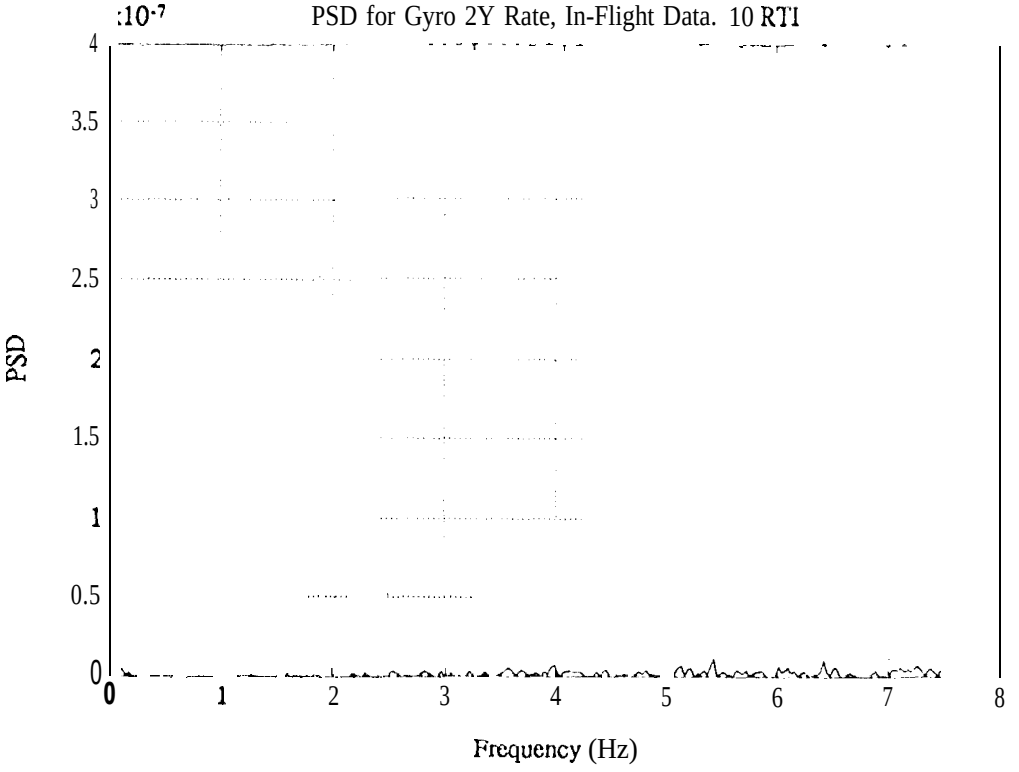


Figure 24. PSD of Gyro 2Y Rate for the In-Flight 10 RTI Excitation Case (Replot Fig. 14(b) Using the Same Scale of Figs. 21-23 and Omitting the Artifact Modes)